2002

A Comparison of Vertical Velocity Profiles from the Balloon Borne Sounding System and the 915/50 MHz Radar Wind Profiler/Radio Acoustic Sounding System to Parcel Theory at the ARM SGP Site

Joshua R. Ravenscraft
Eastern Illinois University

THESIS/FIELD EXPERIENCE PAPER
REPRODUCTION CERTIFICATE

TO: Graduate Degree Candidates (who have written formal theses)

SUBJECT: Permission to Reproduce Theses

The University Library is receiving a number of request from other institutions asking permission to reproduce dissertations for inclusion in their library holdings. Although no copyright laws are involved, we feel that professional courtesy demands that permission be obtained from the author before we allow these to be copied.

PLEASE SIGN ONE OF THE FOLLOWING STATEMENTS:

Booth Library of Eastern Illinois University has my permission to lend my thesis to a reputable college or university for the purpose of copying it for inclusion in that institution's library or research holdings.

[redacted] [redacted]

Author's Signature Date

I respectfully request Booth Library of Eastern Illinois University **NOT** allow my thesis to be reproduced because:

____

____

____

Author's Signature Date

A Comparison of Vertical Velocity Profiles from the Balloon Borne Sounding System and the 915/50 MHz Radar Wind Profiler/Radio Acoustic Sounding System to Parcel Theory at the ARM SGP site.

BY

Joshua R. Ravenscraft

Thesis

SUBMITTED IN PARTIAL FULFILLMENT OF THE REQUIREMENTS FOR THE DEGREE OF

<u>Master of Science in Natural Science</u>

IN THE GRADUATE SCHOOL, EASTERN ILLINOIS UNIVERSITY
CHARLESTON, ILLINOIS

2002
YEAR

I HEREBY RECOMMEND THAT THIS THESIS BE ACCEPTED AS FULFILLING THIS PART OF THE GRADUATE DEGREE CITED ABOVE

[redacted] [redacted]

DATE THESIS DIRECTOR

[redacted] [redacted]

DATE DEPARTMENT HEAD

Department of Physics
Master of Science in Natural Sciences
Physics Concentration
Thesis Acceptance

Title:
A Comparison of Vertical Velocity Profiles from the Balloon Borne Sounding System and the 915/50 MHz Radar Wind Profiler/Radio Acoustic Sounding System to Parcel Theory at the ARM SGP site.

By
Mr. Joshua R. Ravenscraft

The undersigned Thesis Committee hereby recommend that this thesis be accepted as fulfilling part of the Master of Science in Natural Sciences in Physics degree program:

1.[redacted] Date: July 15, 2002

2[redacted] Date: July 15, 2002

3[redacted] Date: July 15, 2002
Dr. A. Douglas Davis

4[redacted] Date: July 15, 2002
Mr. Christopher Klaus

Abstract

In this study we characterized vertical wind velocity profiles in the troposphere using the Atmospheric Radiation Measurement (ARM) equipment facility at the Southern Great Plains (SGP) site in Lamont OK established by the Department of Energy (DOE) and administered through Argonne National Laboratories (ANL). Using the Balloon Borne Radio Sonde (BBSS) system launched four times per day, we collected ambient temperature profiles and lapse rates from the period of June to September of 2001. Concurrently the Rass Radar Wind Profiler collected vertical wind speed data at 915 MHz continuously throughout this period. The BBSS data is visualized using a Skew-T atmospheric profile plot allowed calculations of the Convective Available Potential Energy (CAPE) by integrating from the fiducial saturated adiabatic lapse rate curve to the ambient temperature curve. From this we calculated the vertical velocity using ideal atmospheric parcel theory. In addition the linear Brunt-Väisälä convective parcel theory is compared to the Skew-T derived lapse rate velocities applied to the stable regime. A statistical comparison was made to characterize the condensation fraction associated with vertical winds at the topographically unique SGP location. Robustness of the comparison is tested using second, third and fourth order moments and by testing for a normal distribution of the

deviations. We found that the $\chi^2 = 0.889$ for CAPE and RWP vertical velocities measured in the aggregate. This characterization matches the methodology used at a similar site in Darwin, Australia and was used as input for full scale three-dimensional modeling of the atmosphere over SGP. The CAPE derived vertical wind speed parameter was found to be 0.55 for the SGP site.

Dedication

To my wife Diane,

I love you.

Acknowledgements

I would like to thank my wife for supporting me these last three years. Without her love, patience, and understanding none of this would be possible.

I would like to thank my committee Dr. James McGaughey, Dr. A. Doug Davis, and Mr. Christopher Klaus for taking time out of their busy schedules to read and evaluate my thesis. I would also like to thank Sharon Nichols for all her support.

I would also like the thank my advisor Dr. Keith Andrew who taught me the process of original research and helped me better understand the world around us.

Lastly, I would like to thank all the wonderful people that I have had opportunity to become friends with over these last three years. I would especially like to thank Mark Welter and Julie Johnson for their continuous support throughout the entire process. Thanks.

Table of Contents

List of Figures

List of Tables

Introduction

When and where is the next tornado going to hit? What path will the next hurricane take? Scientists have asked these questions since the beginning of meteorological studies. In the beginning, man thought angry gods caused weather. Even today, there are cultures that pray to gods to bring better weather. As mankind evolved, so did the methods by which weather was observed. During the Golden Age of Greece, Aristotle compiled data that included rain, hail, snow, and other meteorological phenomena in a book titled *The Meteorologica* in 318 B.C. Also during this time Hippocrates wrote a book about how weather affected people's health called *Airs, Waters, &Places* [1].

Following the Golden Age of Greece, science declined as wars for territory increased. It wasn't until the late 1500's and early 1600's during the scientific revolution that new equipment and ideas allowed for scientific advancements in the study of meteorology. The invention of the thermometer by Galileo in 1603 and the barometer by Torricelli in 1643 made data collection more accurate. As time went on, scientists started seeing patterns in the weather data and applied it to their current weather conditions. It was from this data that a more reliable weather prediction system started.

Today most meteorologists use statistical data dating back over 100 years to statistically predict the weather patterns. There have been many advancements in the last few years largely due to the advancement of technology available to them for *in situ* or real time data. The Atmospheric Radiation Measurement (ARM) equipment facility at the Southern Great Plains (SGP) site in Lamont, Oklahoma has the some of the most powerful high-resolution weather gathering instruments available. The SGP site is one of three major sites operated by Argonne National Laboratories (ANL) in conjunction with the Department of Energy (DOE). Equipment such as high resolution Doppler radar allows scientists to see cloud formation and activity from ground level to tens of miles in the air. Along with ground instruments and weather satellites that send images of the atmosphere over specific regions scientists are able to establish better dynamical models of the weather. Scientists around the world are using these new instruments to devise more accurate dynamic models for a particular region. Similar studies are being conducted in Darwin, Australia, Belém, South America, and in California. Analysis of the data is only reliable over the topographical area where the instruments are located. By analyzing the data over the SGP site, a vertical velocity parameter was developed that could help create a better dynamic model of the weather for Lamont, Oklahoma.

Chapter 1: The Atmosphere

To look at the dynamics of an air parcel traveling vertically in the atmosphere it is necessary to look at the atmosphere itself. When compared to the size of the earth the atmosphere is very thin. Most of the mass of the atmosphere is located under the 500-mb level, which is a height of approximately 5.5 km. This is than 0.001 of the radius of the earth [2].

It is important to know the composition of the atmosphere. Since our goal is to analyze severe weather situations, it is important to know exactly how much water vapor is present in the atmosphere that is responsible for this weather. According to Wallace [2] the atmosphere consists of about 76% nitrogen and 23% oxygen by mass, Table (1).

Table 1: [2]

Composition of the earth's atmosphere below 100 km

Constituent	Molecular weight	Content (fraction of total molecules)
Nitrogen (N_2)	28.016	0.7808 (75.51% by mass)
Oxygen (O_2)	32.00	0.2095 (23.14% by mass)
Argon (A)	39.94	0.0093 (1.28% by mass)
Water vapor (H_2O)	18.02	0–0.04
Carbon dioxide (CO_2)	44.01	325 parts per million
Neon (Ne)	20.18	18 parts per million
Helium (He)	4.00	5 parts per million
Krypton (Kr)	83.7	1 parts per million
Hydrogen (H)	2.02	0.5 parts per million
Ozone (O_3)	48.00	0–12 parts per million

As seen in Table (1), the amount of water vapor is roughly 0 to 4 percent of the molecules in the atmosphere. This small amount of water vapor present in the entire atmosphere accounts for all the precipitation on the planet.

The atmosphere has layers where the physical properties of an air parcel behave differently. The lowest layer, called the troposphere, is located between the earth's surface up to a pressure of about 190 mb. "The troposphere (literally, the turning or changing sphere) accounts for more than 80% of the mass and virtually all of the water vapor, clouds, and precipitation in the earth's atmosphere"[2]. Since most of the water vapor resides in the troposphere than most of the earth's weather is generated in the troposphere. As an air parcel rises in the troposphere the temperature of that parcel decreases as shown in Fig. (1). The next layer in the atmosphere is called the tropopause, here a transition takes place between the troposphere and the stratosphere. During this transition the air parcel stays at a steady temperature as it rises into the stratosphere. Fig.(1) shows the temperature increase profile defined by the US Standard Atmosphere, which was established by the National Oceanic and Atmospheric Administration in 1976 as a standard pressure at sea level being 1013 mb [2]. "The stratosphere (literally, the layered sphere) is characterized by very small vertical mixing. Even the most vigorous thunderstorm updrafts are unable to penetrate more than a few kilometers into the lower stratosphere"[2]. One can think of the stratosphere as a lid that keeps the weather contained in the troposphere. One of the main difference between the troposphere and the stratosphere is that as an air parcel rises through the stratosphere its temperature increases and is shown in Fig. (1).

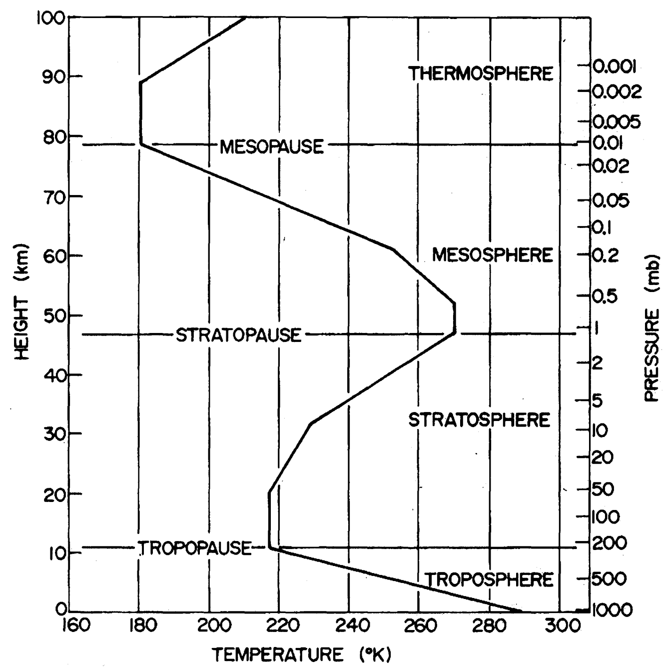

Figure 1: Vertical temperature profile for the U.S. Standard Atmosphere [2].

The reason for the different temperature changes in each level of the atmosphere is directly related to the molecules that are present in each level. Since the troposphere contains nearly all the water vapor in the atmosphere, “it absorbs solar energy and thermal radiation from the planet’s surface” [3] which causes the surrounding air parcel to decrease in temperature. The stratosphere contains virtually no water vapor and nearly all the ozone in the atmosphere. “Ozone plays the major role in regulating the thermal regime of the stratosphere. Temperature increases with ozone concentration. Solar energy is converted to kinetic energy when ozone molecules absorb ultraviolet radiation, resulting in heating of the stratosphere” [3]. In the mesosphere water vapor and ozone are negligible and therefore the temperature is lower than the stratosphere and troposphere. The few molecules that remain the thermosphere increase in temperature as they move vertically. “This increase in temperature is due to the absorption of intense solar radiation by the limited amount of remaining molecular oxygen” [3].

Since weather is contained within the troposphere and the very lower parts of the stratosphere the other layers of the atmosphere are not as critical to this analysis. The layers above the stratosphere are the stratopause, mesosphere, mesopause, and thermosphere. The stratopause, like the tropopause, is the transition layer between the stratosphere and the mesosphere. The mesosphere is comparable to the troposphere because the temperature decreases as air moves up in altitude as well as not inhibiting the motion of the air like the stratosphere. The mesopause is the transition layer between the mesosphere and the thermosphere. The thermosphere extends upward to an altitude of several hundred kilometers and can vary in temperature from 500°K to 2000°K. Not shown in Fig. (1) is the exosphere that extends upward to about 500 kilometers. The exosphere is where the space station and the shuttle orbit the earth.

Chapter 2: Thermodynamics in the Atmosphere

An understanding of thermodynamics is needed to describe physical changes an air parcel undergoes as it moves vertically through the atmosphere. The following summary of the needed thermodynamics follows closely the material in Serway [4] and Reif [5]. Air is composed of many different types of gases. A simple analysis of gas is made possible by a basic equation of state known as the ideal gas law [6]. Therefore a basic approach to analyzing air is to assume it is an ideal gas. An ideal gas is one in which the following assumptions are made: 1-- the temperature of the gas is not low enough to condense into a liquid, 2-- the gas molecules do not interact except upon elastic collisions, and 3-- the molecular volume is negligible compared to the volume of the parcel. The ideal gas law can be expressed as

$$PV = nRT. \tag{2.1}$$

In this equation P is pressure measured in pascals (Pa), V is volume measured in cubic meters (m^3), n is the number of moles, T is temperature measured in Kelvins (K), and R is the universal gas constant which has a value of 8.315 J/mol•K. According to this equation an ideal gas is one in which the ratio of PV/nT is a constant. A kinetic molecular description of the ideal gas law is in terms of the number of molecules N and their interactions and not the number of moles. Substituting for n, Eq.(2.1) becomes

$$PV = Nk_BT. \tag{2.2}$$

Here k_B is Boltzman's constant which is equal to

$$k_B = \frac{R}{N_A} = 1.38x10^{-23} J/K. \tag{2.3}$$

Eq. (2.2) can be expressed in terms of ρ, the density of the gas as

$$P = \frac{\rho k_B T}{M} \tag{2.4}$$

From these equations one can see that the pressure, volume, and temperature are considered to be the thermodynamic variables.

Consider the work done on an ideal gas that occupies a piston with an initial volume V and pressure P, Fig. (2). As the piston moves upward from y to y + dy the volume of the gas increases from V to V + dV.

According to the definition of pressure P = F/A, where F is the force applied perpendicular to a surface of cross-sectional area A. The work done on the gas by the piston is given as

$$dW = Fdy = PAdy. \tag{2.5}$$

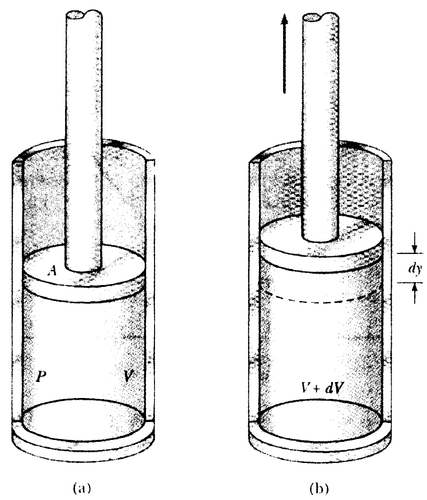

Figure 2: (a) Piston at rest. (b) Piston moving up a distance dy.[4]

Notice that A dy is the increase of the volume dV, so the work done on the gas becomes

$$dW = PdV. \tag{2.6}$$

To find the total work done on the gas through a change of V_i to V_f one can integrate both sides of Eq. (2.6), which gives

$$\Delta W = \int_{V_i}^{V_f} PdV. \tag{2.7}$$

From Eq. (2.6) if the pressure of the gas were to be plotted against the volume of the gas, called a PV diagram, the work done would equal the area under the curve between V_i and V_f, Fig. (3).

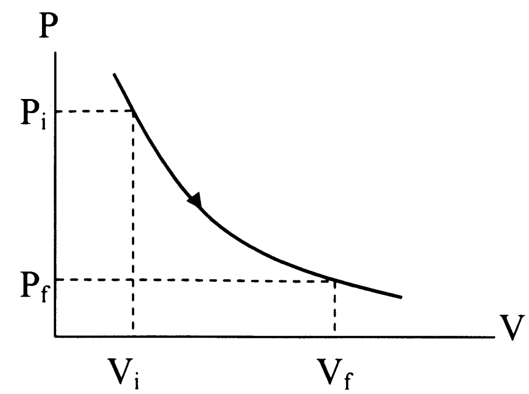

Figure 3: Work is equal to the area under the curve between V_i and V_f on the PV diagram.

The PV diagram is the most basic thermodynamic diagram. We will develop the concept of thermodynamic diagrams further in chapter 5.

Next consider the fundamental laws of thermodynamics, Table (2).

Table 2: Fundamental Laws of Thermodynamics

- Zeroeth Law -- $T_A = T_C$, $T_B = T_C$, $\therefore T_A = T_B$
- 1st Law -- $dU = đQ - đW$
- 2nd Law -- $\Delta S > 0$
- 3rd Law -- $\lim_{T \to T_o} S \to S_0$

The Zeroeth law of thermodynamics states, "if two systems are in thermal equilibrium with a third system, they must be in thermal equilibrium with each other"[5]. The first law states that any change of internal energy dU is equal to the difference between the amount of heat put into the system đQ and the amount of work done by the system đW, Eq. (2.8).

$$dU = đQ - đW \quad (2.8)$$

It is important to know that the quantities $đQ$ and $đW$ represent an inexact differentials which means that the change of heat $đQ$ and the change of work $đW$ depend on the path taken and not only the initial and final states. Whereas dU only depends on the initial and final states of the internal energy.

The second law states that if a system is in equilibrium it has a certain quantity called entropy (S) measured in J K^{-1}, which has the following properties, determined by the environment of the system. First, "in any process in which a thermally isolated system goes from one macrostate to another, the entropy tends to increase"[5],

$$\Delta S \geq 0. \quad (2.9)$$

Second, "if the system is not isolated and undergoes a quasi-static infinitesimal process, which is a process that moves slow enough to keep the parcel in thermal equilibrium at all times, in which it absorbs heat dQ"[5], than

$$dS = \frac{đQ}{T} \quad (2.10)$$

The third law states that the entropy of a system S has a limiting property such that as T goes to T_0, S goes to a constant S_0, where S_0 is independent of all the parameters of that system.

The change of heat dQ of a system can be found by plotting Eq. (2.10) in similar fashion as done with Eq. (2.7) the area under the curve equals the change of heat in the system, Fig. (4).

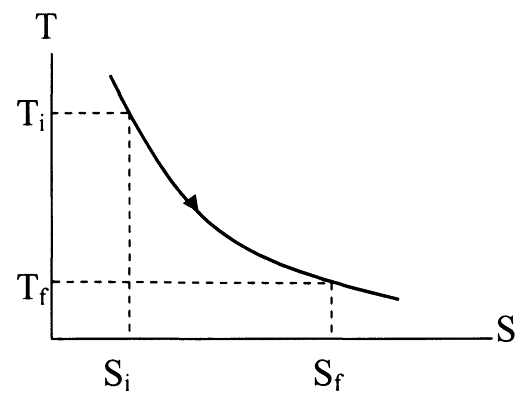

Figure 4: Heat is equal to the area under the curve between S_i and S_f on the TS diagram

There are several processes in thermodynamics that are useful to us which can be investigated through Eq. (2.8). If a process occurs at a constant pressure it is called an isobaric process. In an isobaric process the change of pressure dP = 0 and the work done is equal to

$$\Delta W = P\int_{V_i}^{V_f} dV$$

$$\therefore \Delta W = P\Delta V. \tag{2.11}$$

If a process occurs at a constant volume it is called an isovolumetric or isochoric process. In this process the change of volume of the system dV=0. Since dV = 0, from Eq. (2.6) the total work done on the system is zero since work is directly related to the change of volume. Therefore the change of internal energy comes directly from the amount of heat added or taken from the system, Eq. (2.12).

$$dU = dQ \tag{2.12}$$

If a process occurs at a constant temperature it is called an isothermal process. In this process the change of temperature of the system dT = 0. In an isothermal process the change of internal energy is zero because the "internal energy of an ideal gas is a function of temperature only"[4]. Therefore the amount of heat added to the system is equal to the amount of work done on the system, Eq. (2.13).

$$dQ = -dW \tag{2.13}$$

Finally, if a process occurs in which no heat is added or taken away from the system it is called an adiabatic process. In an adiabatic process the change of heat of the system dQ = 0. Since dQ = 0, the change of internal energy is equal to the negative work done on the system, Eq. (2.14).

$$dU = -dW \tag{2.14}$$

It is this process that will be modeled for the air parcel ascending vertically and will be assumed to rise adiabatically through the air. Fig. (5) shows each of the processes on a PV diagram and the paths that the gas could take.

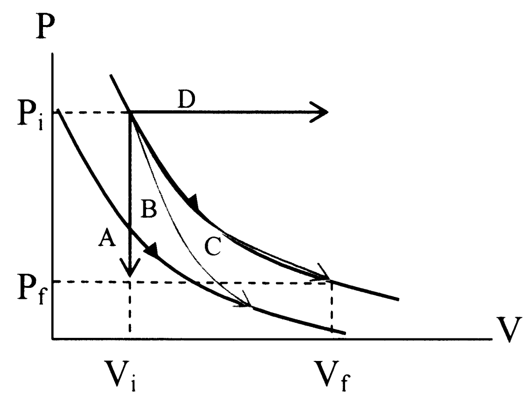

Figure 5: Line A represent an isovolumetric process. Line B represents an adiabatic process. Line C represents an isothermal process. Line D represents an isobaric process.

Chapter 3: Kinetic Theory of Gases

Now that a macroscopic model of an ideal gas has been examined, it is also useful to examine a molecular model of an ideal gas. This summary of the molecular model of an ideal gas follows closely the material in Serway [4] and Sears [7].

In a similar fashion to that of the macroscopic model of an ideal gas, there are some underlying assumptions that need to be made in order to proceed with the molecular model: 1 -- The number of molecules is large and the distance between each molecule is also large. This means that the total volume of the molecules is small compared to that of the container itself. 2 -- Each molecule obeys Newton's three laws of motion where each molecule randomly moves in the container. 3 -- When the molecules collide with the walls of the container and each other they undergo an elastic collision such that energy and momentum are conserved. 4 -- The interactive forces between the molecules are negligible except during collisions. 5 -- The gas under consideration is composed of all the same molecules. With these assumptions we can look at the interactions of the molecules within the container.

Consider a molecule inside a cubic box with sides of length d that collides with one of the walls of the box moving at some velocity **v**, Fig. (6).

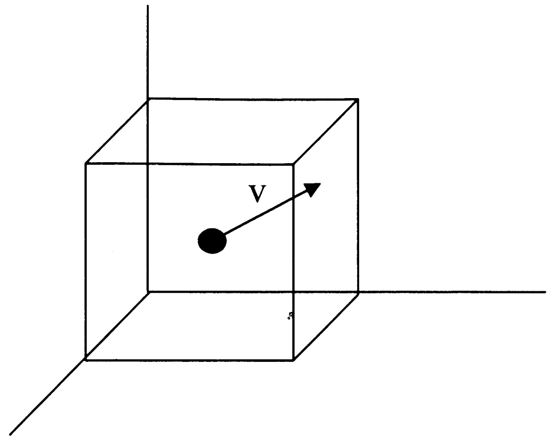

Figure 6: Cubic box in which a molecule is colliding with a wall of the container.

Applying Newton's second law to the molecule colliding with the wall of the box, the force that the wall exerts on the molecule is equal to Eq. (3.1).

$$F_{\text{on wall}} = \frac{mv_x^2}{d} \tag{3.1}$$

If all of the forces exerted on the wall were averaged in the x direction it would give the following, Eq. (3.2).

$$F = \frac{Nm}{d}\overline{v}_x^2. \tag{3.2}$$

Here N is the number of molecules and v-bar is the average of all the velocities in the x direction. If we take this situation and apply it to the x, y, z, directions we find that the total force is equal to Eq. (3.3).

$$F = \frac{N}{3}\left(\frac{m\overline{v}^2}{d}\right) \tag{3.3}$$

The derivations of Eq. (3.1), (3.2), and (3.3) can be found in appendix A. Plugging Eq. (3.3) into the equation P = F/A a value for the total pressure exerted on the walls of the box by the molecules is obtained, Eq. (3.4).

$$P = \frac{F}{A} = \frac{F}{d^2} = \frac{1}{3}\left(\frac{N}{d^3} m\overline{v}^2\right) = \frac{1}{3}\left(\frac{N}{V} m\overline{v}^2\right)$$

$$P = \frac{2}{3}\left(\frac{N}{V}\right)\left(\frac{1}{2} m\overline{v}^2\right) \tag{3.4}$$

This result indicates that the pressure is proportional to the number of molecules per unit volume and directly proportional to the average kinetic energy of the molecules.

Taking Eq. (3.4) and Eq. (2.2) we can find the average kinetic energy of the molecules with respect to temperature as

$$\frac{1}{2} m\overline{v}^2 = \frac{3}{2} k_B T. \tag{3.5}$$

Eq. (3.5) also represents the total energy of a monatomic gas since a monatomic gas molecule moves only in the x, y, and z directions. Therefore, it is said to have three degrees of freedom. Dividing the right side of Eq. (3.5) by 3, each degree of freedom has energy of $1/2k_BT$. If the gas consists of diatomic molecules there are more possible degrees of freedom. These degrees of freedom can come from the rotational or vibrational energies that a diatomic molecule can obtain. Rotationally the diatomic molecule can rotate three different ways, but only two of the rotations are substantial enough to add to the total energy. Vibrationally the diatomic molecule has two degrees of freedom, back and forth, which adds to the total energy. Adding all the degrees of freedom for a diatomic molecule the total energy of the system becomes

$$E_T = \frac{7}{2} N k_B T = \frac{7}{2} nRT. \tag{3.6}$$

Consider an ideal gas in which one wants to change the temperature of the system. This temperature change can take places using different paths as shown in Fig. (7). Since ΔT is the same for each of these paths, the change of internal energy is also the same for each one. However, according to Eq. (2.8) the amount of heat added to the system equals the change of internal energy plus the work done. The work done on each of the paths in Fig. (7) is different from the earlier explanation that work is equal to the area under the curve on a PV diagram.

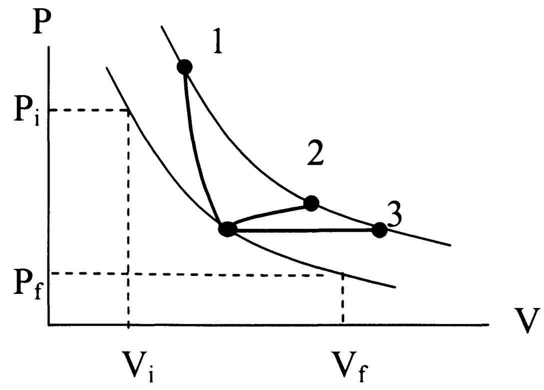

Figure 7: An ideal gas is taken from one isotherm to another following three different paths.

Since this occurs, it requires the definition of a new term called molar specific heat for the two processes that occur most frequently, which are the constant volume and pressure processes as discussed in Ch.(2) . Using the definition of molar specific heat, the amount of heat required to change the temperature of a system is

$$Q = nC_V dT \text{ (constant volume)} \tag{3.7}$$

$$Q = nC_P dT \text{ (constant pressure)} \tag{3.8}$$

where C_V and C_P are the molar specific heat at constant volume and pressure respectively. Applying Eq. (3.7) to a monatomic gas which undergoes an isovolumetric expansion, the molar specific heat can be defined in terms of internal energy dU. In an isovolumetric expansion the work done dW is zero, such that all heat Q added to the system changes into U, Eq. (2.12).

Setting Eq. (2.12) equal to Eq. (3.7) the molar specific heat at a constant volume is

$$C_V = \frac{1}{n}\frac{dU}{dT}. \tag{3.9}$$

Instead of taking the gas through an isovolumetric process, suppose the gas is taken through an isobaric process. As Eq. (2.11) shows, the work done is equal to the pressure and the change of volume. This leads to an internal energy equation

$$dU = đQ - đW = nC_P dT - PdV. \tag{3.10}$$

Rearranging Eq. (3.9) and substituting in for dU and PdV = nRdT from the ideal gas law a relationship exists between C_V and C_P

$$\begin{aligned} nC_V dT &= nC_P dT - nRdT \\ C_P - C_V &= R. \end{aligned} \tag{3.11}$$

Suppose now the gas is taken through an adiabatic process in which no heat is gained or lost. In this case the pressure and the volume are related at any time during this process by the equation

$$PV^{\gamma} = \text{constant} \tag{3.12}$$

where $\gamma = C_P/C_V$ is constant throughout the process. Since Eq. (3.12) is a constant throughout the entire adiabatic process, initial and final equations for the system can be written both in terms of P-V and in terms of V-T as

$$P_i V_i^{\gamma} = P_f V_f^{\gamma} \tag{3.13}$$

$$T_i V_i^{\gamma-1} = T_f V_f^{\gamma-1}. \tag{3.14}$$

Chapter 4: Air Parcel

"Many of the most interesting meteorological phenomena are associated with strong or even violent vertical motion. These phenomena suggest that we attempt to determine the conditions that will yield strong vertical motions. The classical approach to this problem is to investigate what will occur when a small parcel is vertically displaced from its original position" [11].

The air parcel mentioned above is defined as an amount of air that is large enough to contain millions of molecules so pressure and density are well defined. However, the parcel must also be small enough so that density and pressure throughout is uniform. "Thus the pressure and density are macroscopic descriptions of the molecular properties and motions of the gas, and the velocity of the parcel is the average of all the molecular velocities" [11]. There are two assumptions that must be made when choosing an air parcel to analyze: 1 -- The pressure of the air parcel will always match the pressure of the surrounding air. 2 -- The parcel moves adiabatically so that the potential temperature is constant throughout the motion. The remainder of this chapter will be focused on the analysis of an air parcel by different methods that develop in Dutton [11] and Wallace [2].

Fig. (8) shows an air parcel in a vertical column of the atmosphere.

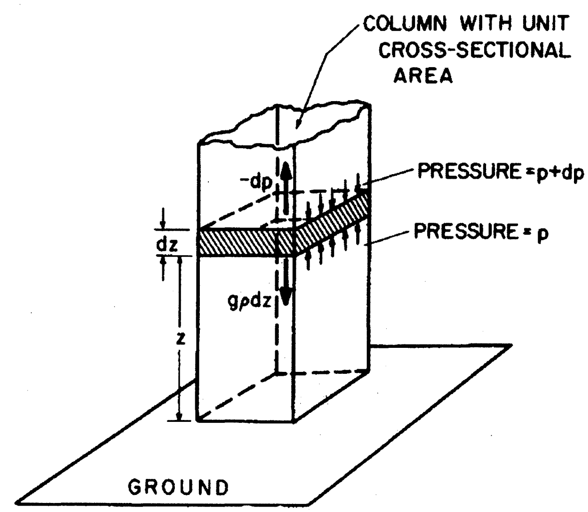

Figure 8: Representation of an air parcel in a vertical column of the atmosphere. [2]

The mass per area of the air parcel is given by ρ dz and the pressure acting on the air parcel due to its weight is equal to ρg dz. The pressure on the top of the air parcel decreases by an amount of dp over a height dz. One must assume that the air parcel is in equilibrium by summing up the forces acting on the parcel of air according to Newton's second law,

$$p_{bottom} = p_{top} + dp \tag{4.1}$$

Since the air parcel is in equilibrium, the forces must equal zero. However, Eq. (4.1) gives a net buoyant force in the positive vertical direction equal to dp. To reach equilibrium, dp must be equal to the pressure acting on the air parcel due to its weight.

$$dp = -g\rho dz$$

$$\frac{dp}{dz} = -g\rho. \qquad (4.2)$$

Eq. (4.2) is known as the hydrostatic equation. Integrating both sides of Eq. (4.2)

$$-\int_{p(z)}^{p(\infty)} dp = \int_{z}^{\infty} g\rho dz$$

$$p(z) = \int_{z}^{\infty} g\rho dz \qquad (4.3)$$

shows that the pressure at a height z will be equal to the weight of air in the vertical column above the parcel. At sea level the pressure equals 1.013 x 10^5 Pa or 1013 mb [2]. The hydrostatic equation "almost always gives an adequate representation between pressure and density makes it a potent concept, especially for analysis of large-scale flow. It provides one relation between p and ρ and the equation of state provides another between p, ρ, and T, and hence one may be eliminated" [11].

Substituting the ideal gas law into Eq. (4.2) with the assumption that the acceleration of gravity is constant throughout the atmosphere by integrating one can obtain the Law of Atmospheres

$$P = \frac{\rho k_B T}{m} \Rightarrow \rho = \frac{Pm}{k_B T}$$

$$\frac{dp}{dz} = -g\left(\frac{Pm}{k_B T}\right) \Rightarrow \int_{p(0)}^{p(z)} \frac{dp}{P} = \int_0^z -\frac{gm}{k_B T} dz$$

$$P(z) = P(o)e^{-mgz/k_B T}. \tag{4.4}$$

The hydrostatic equation assumes a uniform acceleration of gravity as an air parcel moves vertically in the atmosphere. It is important to note that the acceleration due gravity decreases as a function of height by

$$g(\phi, z) = g_\phi \left(\frac{a}{a+z}\right)^2 \tag{4.5}$$

where a is the radius of the earth, z is the height above sea level, and g_ϕ depends on latitude and is given by the equation

$$g_\phi = 980.6160[1 - 2.64x10^{-3} \cos 2\phi + 5.9x10^{-6} \cos^2 2\phi]\ \mathrm{cm/s}. \tag{4.6}$$

If we take a unit mass and raise it to a height z above the earth's surface, the mass has some potential energy equal to the amount of work done against earth's gravitational field. Using Eq. (4.5) with the above statement, the potential energy of a unit mass, known as geopotential, can be expressed by

$$\Phi = \int_0^z g_\phi \left(\frac{a}{a+z}\right)^2 dz + \Phi(0) \tag{4.7}$$

The value for $\Phi(0)$ is usually taken to be zero at sea level. Therefore Eq. (4.7) becomes

$$\Phi(z) = g_\phi \frac{az}{a+z}. \tag{4.8}$$

It is also helpful in meteorology to define levels in the atmosphere where the geopotential is constant. Geopotential height (Z) is used frequently as a vertical component of the atmosphere when energy plays an important role. Geopotential height is defined by

$$Z = \frac{\Phi}{g_o} \quad g_o = 9.80 m/s^2. \tag{4.9}$$

Potential temperature θ is often used in analyzing air parcels rather than actual temperature. Potential temperature is defined as the "temperature which the parcel of air would have if it were expanded or compressed adiabatically from its existing pressure and temperature to a standard pressure p_o" [2]. The equation which defines potential temperature is known as Poisson's equation which is

$$\theta = T\left(\frac{p_o}{p}\right)^{R/C_P}. \tag{4.10}$$

For dry air, $R = R_d = 287$ J deg^{-1} kg^{-1} and $C_P = 1004$ J deg^{-1} kg^{-1}; so $R/C_P = 0.286$ [2]. Potential temperature is an important parameter in meteorology because air parcels often undergo processes which are close to adiabatic, which means that θ remains constant.

The change in temperature of an air parcel as it moves vertically in the atmosphere is called the lapse rate,γ, and is defined by

$$\gamma = -\frac{dT}{dz}. \tag{4.11}$$

The negative sign in Eq. (4.11) gives a positive lapse rate since temperature decreases with height and the units are deg km^{-1}. For a dry parcel of air, the lapse rate γ_d is defined by

$$\gamma_d = \frac{g}{C_p} \cong 10 deg/km. \tag{4.12}$$

This value is only for a dry parcel of air that is being lifted adiabatically. "The actual lapse rate of temperature in the atmosphere, as measured by a radiosonde, averages 6 – 7 deg km^{-1} in the troposphere but it takes on a wide range of values at individual locations" [2].

The mixing ratio is the amount of water vapor in the air compared to the mass of dry air,

$$w \equiv \frac{m_v}{m_d}. \tag{4.13}$$

The mixing ratio w is usually expressed in terms of grams of water vapor to kilograms of dry air. If the air becomes saturated then Eq. (4.13) becomes

$$w_s = \frac{m_{vs}}{m_d} \tag{4.14}$$

where m_{vs} is the amount of water vapor in the saturated air.

The relative humidity RH of the air depends upon both w and w_s. It is the ratio of the actual mixing ratio to the saturated mixing ratio given by

$$RH \equiv 100\frac{w}{w_s}. \tag{4.15}$$

The dew point temperature T_d is a temperature that determines the saturation point of an air parcel. If the air parcels cools to T_d, then the air parcel becomes saturated. Comparably it is when the saturation mixing ratio w_s equals the actual mixing ratio w and the relative humidity becomes 100%.

Using Archimedes's principle the net force F on an air parcel is the difference between the force of gravity on the air parcel of mass M_P and the mass M of the surrounding air displaced by the parcel. This force is assumed to act positively upward given by

$$F = g(M - M_P). \tag{4.16}$$

This force becomes equal to the acceleration of the air parcel when it is applied to Newton's 2nd law of motion

$$M_P \frac{d^2z}{dt^2} = F = g(M - M_P). \tag{4.17}$$

Dividing both sides of Eq. (4.17) by the volume of the air parcel, Eq. (4.17) can be written in terms of the difference of densities of the air parcel and the surrounding air,

$$\frac{d^2z}{dt^2} = g\left(\frac{\rho - \rho_P}{\rho_P}\right). \tag{4.18}$$

Eq. (4.18) shows that if the air parcel is less dense than the surrounding air it will accelerate upward, and if the air parcel is denser then the surrounding air then it will accelerate downward. With the assumptions associated with using an air parcel and the ideal gas law, Eq. (4.18) can also be expressed as

$$\frac{d^2z}{dt^2} = -g\left(\frac{T - T_P}{T_P}\right) = -g\left(\frac{\theta - \theta_P}{\theta_p}\right) \tag{4.19}$$

Dividing Eq. (4.17) by the volume of the air parcel Newton's second law can be rewritten in terms of the change in density between the air parcel and the surrounding air

$$\begin{aligned} F &= g(M - M_P) \\ \rho a &= -g d\rho. \end{aligned} \tag{4.20}$$

Applying the chain rule to Eq. (4.20) gives

$$\rho a = \rho \frac{d^2z}{dt^2} = -g \frac{d\rho}{dz} dz. \tag{4.21}$$

Substituting the result from Eq. (4.19) and Eq. (2.4), Eq. (4.21) can be rewritten into a second order differential equation using the difference of lapse rates between dry air and the actual lapse rate of an air parcel

$$\frac{d^2}{dt^2}\Delta z + \frac{g}{T}(\gamma_d - \gamma)\Delta z = \frac{d^2}{dt^2}\Delta z + \omega^2 \Delta z = 0. \qquad (4.22)$$

A second order differentiation is considered a harmonic oscillator when given in the form of Eq. (4.22). The quantity ω is known as the Brundt-Väisälä frequency, where

$$\omega = \sqrt{\frac{g}{T}(\gamma_d - \gamma)} \qquad (4.23)$$

Eq. (4.23) allows us to determine the period for which the air parcel is rising and falling given by

$$\tau = \frac{2\pi}{\omega} = 2\pi\sqrt{\frac{T}{g}\frac{1}{(\gamma_d - \gamma)}} \qquad (4.24)$$

Knowing the height over which it is oscillating, the velocity of the air parcel can be calculated from Eq. (4.24) by

$$v = \frac{\Delta z}{2\pi\sqrt{\frac{T}{g}\frac{1}{(\gamma_d - \gamma)}}} \qquad (4.25)$$

A more complex way to analyze an air parcel is to apply the Navier-Stokes equations to an air parcel, Table (3).

Table 3: Navier-Stokes Equations

$$\frac{d\vec{v}}{dt} = -\frac{1}{\rho}\nabla p - g\frac{\mathbf{r}}{r} + \frac{1}{\rho}[\nabla \bullet (\mu \nabla \vec{v}) + \nabla(\lambda \nabla \bullet \vec{v})] \tag{4.26}$$

$$c_V \frac{dT}{dt} + p\frac{d}{dt}\left(\frac{1}{\rho}\right) = q + f \tag{4.27}$$

$$\frac{dp}{dt} + \rho \nabla \bullet \vec{v} = 0 \tag{4.28}$$

$$P = \rho R T \tag{4.29}$$

Eq. (4.26) is Newton's second law of motion. The left side of the equation equals the acceleration of the air parcel in three dimensions. Examination of the terms on the right side of Eq. (4.26) is more complex. The first term on the right of the equals sign represents the pressure gradient force. This force is the same force that was used in the hydrostatic equation and in the solution of the Brunt-Väisälä equation. The next term in the equation, -g/r **r**, is the force of gravity on the air parcel itself. The g in this equation is that given by Eq. (4.4) that varies with height and latitude on the earth. The final part to Eq. (4.26) is the force of friction due to the collisions between the molecules in the air. The values of μ and λ are the viscosities of the air molecules.

Eq. (4.27) consists of the Laws of Thermodynamics combined. The terms q and f on the right hand side of the equation refer to the heat lost by the thermodynamic processes and the frictional forces between the molecules respectively.

Eq. (4.28) is called the Continuity Equation. This equation relates the time rate of change of density, and the volume as the air parcel travels through the atmosphere. As the parcel increases in velocity, the density of the parcel increases because the volume decreases. As the velocity decreases the density of the parcel decreases because the volume increases. This follows from Bernoulli's law of pressure. Eq. (4.29) is the ideal gas law written in terms of the density of air, R, and T.

These equations can be deceiving since at first glance there only appear to be four equations. However, since Eq. (4.26) contains a vector quantity **v**, there are three different equations that are derived from that one equation.

The Navier-Stokes equations are the fundamental equations that govern weather. However, since these are non-linear equations that occur in three dimensions it is impossible to solve these equations as a whole for any situation. Instead certain assumptions can be made to the equations that eliminate sections of Eq. (4.26). These assumptions are that the frictional forces are small enough to be negligible and that the force of gravity does not vary with height. If these assumptions are made, then Eq. (4.26) is reduced to a linear equation that depends only on pressure differences. These pressure differences have already been examined in the hydrostatic equation and the Brunt-Väisälä frequency equation. It is on these assumptions that the theoretical values of vertical velocity depend on.

Chapter 5: Thermodynamic Diagram and Skew-T/Log P Plot

The thermodynamic diagram simplifies lengthy calculations and allows meteorologists to determine temperature and humidity changes in the atmosphere. The diagram also quantitatively answers questions regarding things such as how much rain can fall in a given storm or how high a parcel of air has to be lifted to produce a cloud [8]. A basic understanding of the thermodynamic diagram allows further analysis of a more complex thermodynamic diagram called the Skew-T/Log P plot. Some guidelines for reading a thermodynamic diagram are listed below and refer to Fig. (9) found on the proceeding page. The information shown below follows Gedzelman [8].

The horizontal axis of the thermodynamic diagram is used to represent the temperature of a parcel of air in degrees Celsius, while the vertical axis of this graph represents pressure in millibars. As the air parcel moves upward notice that the pressure is decreasing more rapidly at first, then slower as the air parcel moves higher reaching thermal equilibrium as suggested by the laws of thermodynamics.

The black dotted lines that are approximately horizontal are used to indicate altitude in kilometers. These lines, however, are only approximations based on two assumptions [8]: 1-- the sea level pressure is

1013 mb and 2 -- the temperature of the atmosphere decreases 6.5°C per kilometer, which is the lapse rate for a saturated parcel of air.

As an unsaturated parcel of air is lifted it moves up the solid black dry adiabatic lines that slope downward almost at a 45° angle. As a dry air parcel is lifted it follows the slope of the dry adiabat. The dry adiabatic lines are also lines of constant potential temperature and are given in degrees Kelvin.

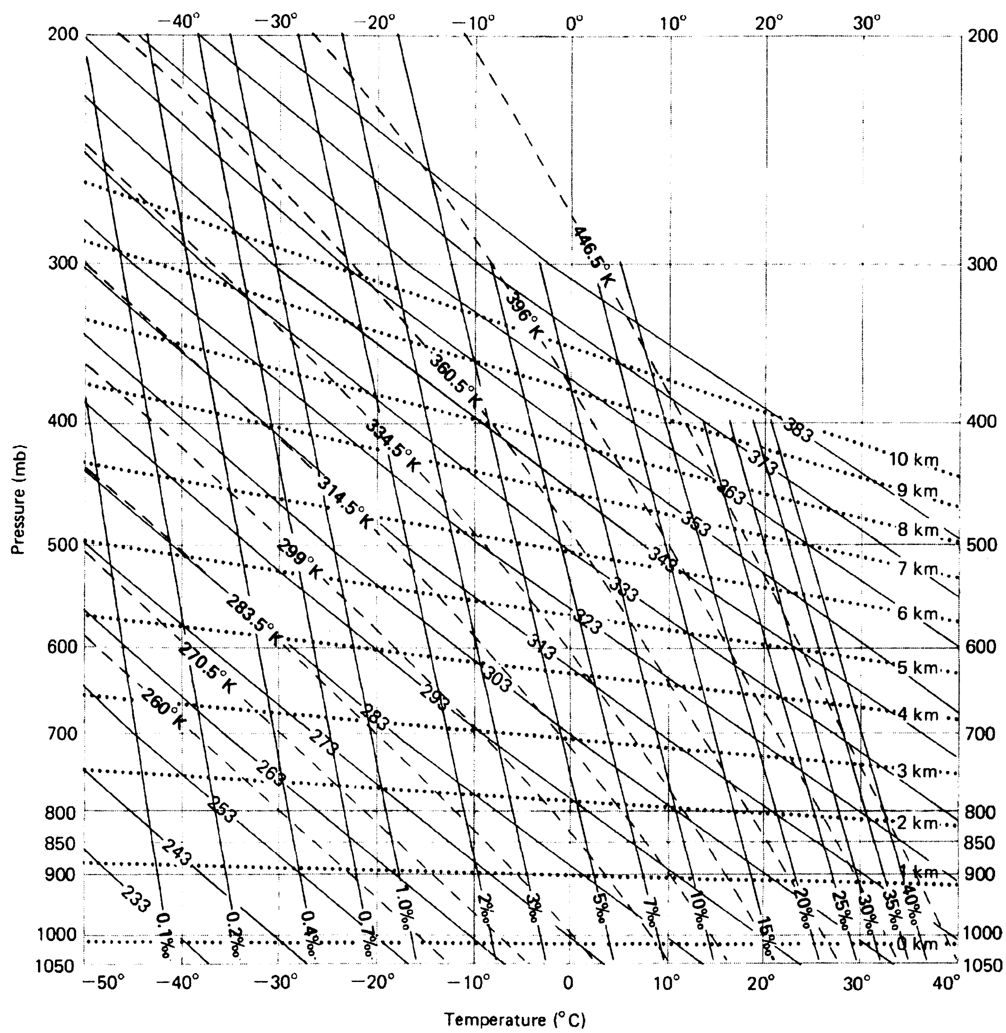

Figure 9: Thermodynamic Diagram [8]

The solid red lines that are almost vertical show how the dew point changes as the air parcel is raised or lowered in the atmosphere. These lines also tell the mixing ratio of air when the dew point is known, as well as the saturated mixing ratio when the temperature is known. Once the air has become saturated (the point where the dry adiabatic line and the dew point line meet) it follows the moist adiabatic line. This line is represented by the dashed red line and shows the lapse rate as the air parcel is raised or lowered once saturation has occurred.

The thermodynamic diagram has numerous applications for meteorologists, such as finding information about the temperature (T), dew point temperature (T_d), and the wet bulb temperature (T_w). If two of the three temperatures are known, finding the relative humidity RH and estimating the amount of precipitation are possible from this diagram.

A more useful thermodynamic diagram often used by meteorologists is called the Skew-T/Log-P diagram, Fig (10). The diagram gets its name from the skewed temperature axis that runs at a 45° angle starting from the bottom left to the top right. The vertical axis is a measure of the log of the pressure because, as a parcel of air climbs in altitude the pressure of the parcel drops logarithmically [4].

The vertical axis is a measure of pressure while the diagonal solid black lines are a measure of temperature, Fig. (10).

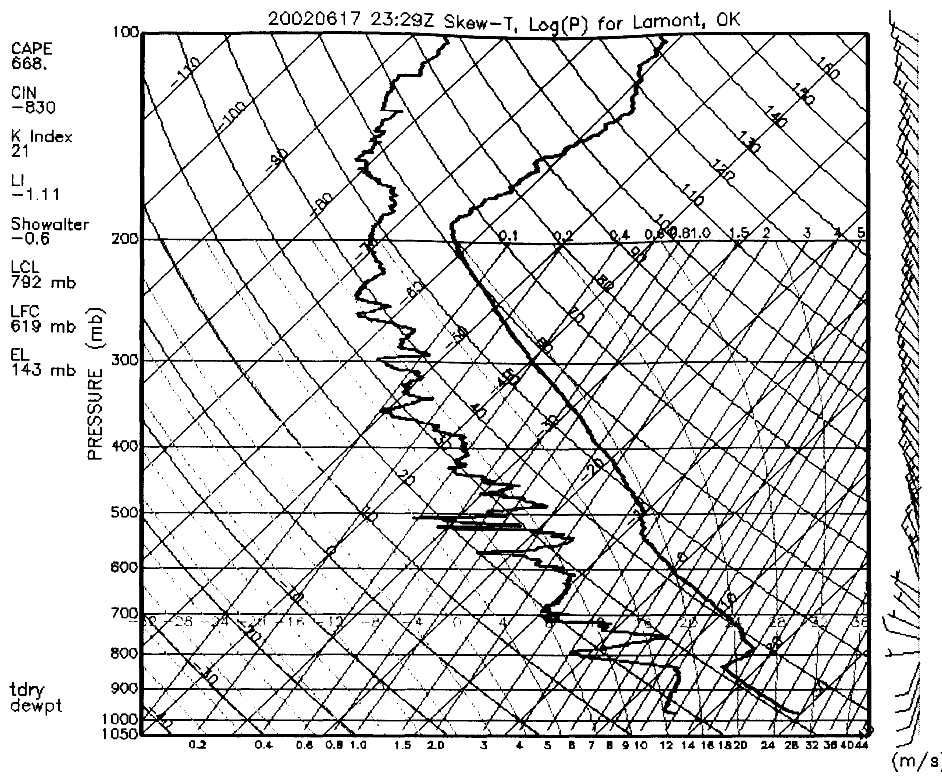

Figure 10: Skew-T/Log-P Diagram [9]

The red lines which start at the bottom and rise diagonally to the left represent the dry adiabatic lapse rate [10]. These lines represent the path of a dry parcel of air as it is raised or lowered in the atmosphere. As in the case of the thermodynamic diagram previously discussed, the numbers that appear above the red lines are the values of the potential temperature, which is the temperature of a any parcel at 1000 mb, if the parcel was moved adiabatically to a pressure of 1000 mb [8].

The green line represents the saturated adiabatic lapse rate that is the path the air parcel travels when it is saturated. Notice that the saturated adiabatic lapse rate line stops around 200 mb. This is due to the fact that as the saturated parcel of air rises it will eventually lose all of the moisture in the parcel and continue rising at the dry adiabatic lapse rate.

The blue lines that start at the bottom of the diagram and rise diagonally to the right represent the mixing ratio. The saturated mixing ratio is the number of grams of water divided by the number of kg of saturated air [8].

The last two lines represent the direct measurements taken from the radiosonde, which is the instrument attached to the weather balloon. The blue line represents the dew point temperature and the red line is the actual temperature of the air. Usually, these lines never intersect except in extremely moist situations.

Along with the graph itself, the Skew-T/Log-P diagram comes with more information attached. On the far right hand side of the diagram are the wind barbs that show the horizontal wind speed for the altitude that the radiosonde is at, Fig. (10). On the right hand side of the diagram is a list of indices that include but not limited to: convection available potential energy (CAPE), normalized convection available potential energy (NCAPE), K index, lifted index (LI), Showalter index (SI), lifted condensation level (LCL), level of free convection (LFC), and the equilibrium level (EL) which will be discussed in more detail in Ch. (6).

Chapter 6: Indices

One of the methods that meteorologists use to predict weather is numerical numbers known as indices. These indices range from a very trivial mathematical calculation to an integration taking over a section of the troposphere. These indices often appear on the Skew-T/Log-P diagrams. There are numerous indices to analyze, but will be limited to the Lifted Index, the Showalter index, the K Index, CAPE, and NCAPE.

The Lifted Index or LI is the most simplistic of the indices that will be examined. It is the difference between the ambient air temperature at 500 mb and the air parcel's temperature if lifted adiabatically from the surface to the lifted condensation level and then moist adiabatically to 500 mb [10]. A parcel's lifted condensation level (LCL) is the level at which clouds start to occur. It usually occurs at the intersection between the temperature and the dew point.

The Showalter Index or SI is very similar to that of the LI. It is the difference between the temperature of the environment at 500 mb and the air parcel's temperature if lifted from 850 mb to the LCL and then moist adiabatically to 500 mb. The SI provides an estimate of the air parcels instability based on the difference of temperatures [10].

The K Index is another method of weather prediction that uses more temperature points than the LI and SI. The K Index equation is

$$K = T_{850} - T_{500} + T_{d850} - (T_{700} - T_{d700}) \qquad (6.1)$$

where the subscript d represents the dew point temperatures at the given pressure values.

Convective Available Potential Energy or CAPE is the area on a thermodynamic diagram enclosed by the environmental temperature profile and the moist adiabat connecting the level of free convection (LFC) to the equilibrium level (EL) [12,13]. CAPE is derived from Eq. (4.17). Integrating both sides it gives

$$E = g \int_{LFC}^{EL} \left(\frac{\theta_P - \theta}{\theta} \right) dz \qquad (6.2)$$

where E is the amount of energy per unit mass or J kg^{-1}. The LFC is the pressure level in which the air parcel becomes unstable and experiences a positive buoyant force. EL is the level in which the air parcel regains stability and experiences a negative buoyant force. Knowing the CAPE of an air parcel and using the conservation of energy, the speed of the air parcel can be determined by

$$\frac{1}{2} m v^2 = CAPE$$

$$v = \sqrt{2 * CAPE} \qquad (6.3)$$

where the velocity is measured in m s^{-1} and the kinetic energy is associated with a unit mass. Meteorologists use certain values of CAPE to help predict the possibility of storms as shown in Table (4).

Table 4: CAPE Guide to Weather [12,14]

CAPE < 0 = Stable

0-1000 = Marginally Unstable (Possible Thunderstorms)

1000-2500 = Moderately Unstable (Possible Severe Thunderstorms)

2500-3000 = Very Unstable (Severe Thunderstorms and possible Tornadoes)

CAPE > 3000 = Extremely Unstable (Catastrophic)

The CAPE values above 1000 will be analyzed further in the paper for accuracy regarding thunderstorm activity.

The Normalized CAPE or NCAPE is the last index that will be discussed. NCAPE is related to CAPE by

$$\text{NCAPE} = \frac{\text{CAPE}}{\text{FCL}}. \tag{6.4}$$

FCL is called the free convection level and is found by the difference of altitudes between the EL and the LFC [15]. The NCAPE is takes into account the height over which the CAPE occurs which gives a more precise estimate for weather forecast. Table (5) is a summary of a study in Northern California of NCAPE and severe weather.

Table 5: NCAPE Guide to Weather [15]

NCAPE<0.03 = Isolated to scattered showers occurred

0.04 - 0.08 = Numerous showers, scattered thunderstorms

0.09 - 0.13 = Numerous thunderstorms, isolated to scattered strong thunderstorms

NCAPE > 0.14 = Strong thunderstorms

Chapter 7: Instruments

To compare vertical wind velocities for severe weather, data from three different instruments were used. These instruments supplied information regarding CAPE, vertical wind velocities, horizontal wind velocities, and precipitation output. The most essential of the three instruments was the Balloon-Borne Sound System (BBSS).

The BBSS has two main components to the system. The first component is a disposable Väisälä radiosonde. The radiosonde is comprised of different instruments for collecting various quantities of data. The instruments that make up the radiosonde are a thermistor which measures temperature, a hygristor which measures relative humidity, an aneroid barometer which measures pressure, a baroswitch which is a switching mechanism for the barometer, a commutator bar which transmits humidity and reference information as well as temperature information, an oscillator radio transmitter, and a battery [16]. The box is attached to a balloon that is made of a thin film or rubber as shown in Fig. (11).

At launch, the balloon is filled with helium to a diameter of about two meters. As the balloon rises the diameter expands to about eight meters before the balloon bursts. As the balloon rises through the air the radiosonde takes data on the thermodynamic state of the atmosphere, the wind speed

Figure 11: Balloon Borne Sounding System being released [17]. (Photo credit- Dr. Bill Rose of Michigan Technical University)

and the direction. The primary quantities that are measured from the BBSS during a free balloon ascent as a function of time are listed below in Table (6).

Table 6: Primary quantities measured by the BBSS [18]

- Pressure (hPa)
- Temperature (°C)
- Relative Humidity (%RH)
- Wind speed (m/s)
- Wind direction (deg)

The secondary or derived quantities that are measured from the BBSS during a free balloon ascent also as a function of time are listed below in Table (7).

Table 7: Secondary quantities measured by the BBSS [18]

- Altitude (gpm)
- Dew Point (°C)
- Ascent Rate (m/s)
- Latitude of Sonde (°N)
- Longitude of Sonde (°W)
- u-component of wind velocity (m/s)

The second component of the BBSS is the ground station to which the data is sent back from the radiosonde as it ascends through the atmosphere. The ground station at the SGP site consists of a receiver processor, a UHF receiver, a GPS processor, a UHF antenna, a GPS antenna, and a floppy disk drive. Once the data is received from the radiosonde, the information is then plotted as a thermodynamic diagram called a Skew-T plot.

While the radiosondes are very durable, there are situations that occur which interfere with the quality of data. Some of the more common situations that the BBSS might experience which can affect the quality of the data received are incorrect surface conditions, humidity sensor saturation or icing, and interference and signal confusion with other radiosondes [18].

The second instrument that was used to compare the results was the Radar Wind Profiler and RASS 50 MHz and 915 MHz (RWP50 and RWP915). The RWP50 consists of a large antenna field of elements created essentially by coaxial cable suspended roughly 1.5 m above a ground plane. The approximately 70 m square antenna is oriented in a horizontal plane so the "in-phase" beam travels vertically as shown in Fig. (12).

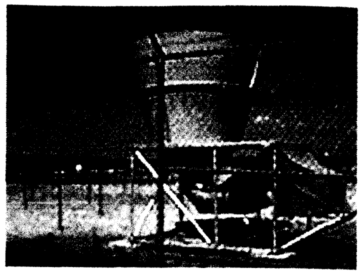

Figure 12: RWP50 [19]

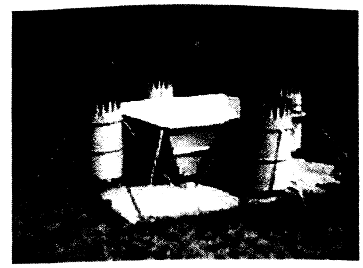

Figure 13: RWP915 [20]

The RWP915 is constructed of an antenna that is approximately 4 m square and is oriented horizontally so the "in-phase" beam travels vertically as shown in Fig. (13). Along with the horizontal antenna the each system includes acoustic sources, a mobile acoustic source, a receiver, an interface module, and a computer for data analysis and processing.

"The RWP50 measures wind profiles from (nominally) 2 to 12 km and virtual temperature profiles from 2 to 4 km" [19]. "The RWP915 measures wind profiles from (nominally) .1 km to 5 km and virtual temperature profiles from .1 km to 1.5 km" [20]. The primary measurements of both the RWP50 and the RWP915 are the intensity and Doppler frequency of backscattered radiation. The more interesting data received from the RWP instruments are the secondary measurements derived from the primary quantities. These measurements include horizontal wind speeds and direction, vertical wind speeds, and virtual temperature as a function of height. The accuracy to which the RWP50 and the RWP 915 collect data for horizontal wind speed is 1.5 m/s, for vertical wind speed is 0.75 m/s, and for virtual temperature is 0.5 degrees [17,18].

The third instrument used was the Surface Meteorological Observation System (SMOS). The SMOS mostly uses conventional in situ sensors to obtain 1 minute and 30-minute averages of surface wind speed, wind direction, air temperature, relative humidity, barometric pressure, and precipitation. The data that was most relevant to the measurements was the precipitation data. The precipitation gauge is an electrically heated, tipping bucket precipitation gauge manufactured by NovaLynx as shown in Fig. (14). The precision of the precipitation data is 0.245 +/- 0.254 mm. According to the manufacturer of the tipping-bucket rain gauge, for rain less then 75 mm per hour with light to moderate winds, the collection efficiency of the gauge is 99 to 100%. However, during heavy storms or strong winds, the collection efficiency is reduced. Manufacturers have not attempted to specify accuracy for these conditions.

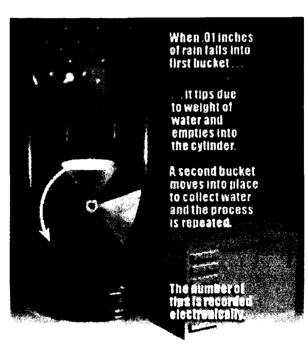

Figure 14: Tipping bucket precipitation gauge. [21]

The last instrument that was used was the Millimeter Wave Cloud Radar (MMCR). The purpose of using the MMCR is to determine if there were clouds on the particular days of measurement and where the cloud boundaries were. The radar also reports radar reflectivity of the atmosphere up to 20 km and possesses a Doppler capability that allows the measurement of cloud constituent vertical velocities. The MMCR operates at a frequency of 35GHz and has a Doppler resolution of less than 0.1 m/s [22].

Chapter 8: Data

As seen from Eq. (6.3) the vertical velocity of an air parcel should equal

$$v = \sqrt{2 * CAPE}. \tag{8.1}$$

From the Brunt-Väisälä frequency the velocity of an air parcel should equal, Eq. (4.22) [23]

$$v = \frac{\Delta z}{2\pi\sqrt{\frac{T}{g}\frac{1}{(\gamma_d - \gamma)}}}. \tag{8.2}$$

A quantitative statistical comparison between the theoretical values of vertical velocity and the direct measurement of vertical velocity by the RWP provides insight on how accurate the theoretical models can predict the weather. A typical sample of the data from the RWP is shown in Fig. (15).

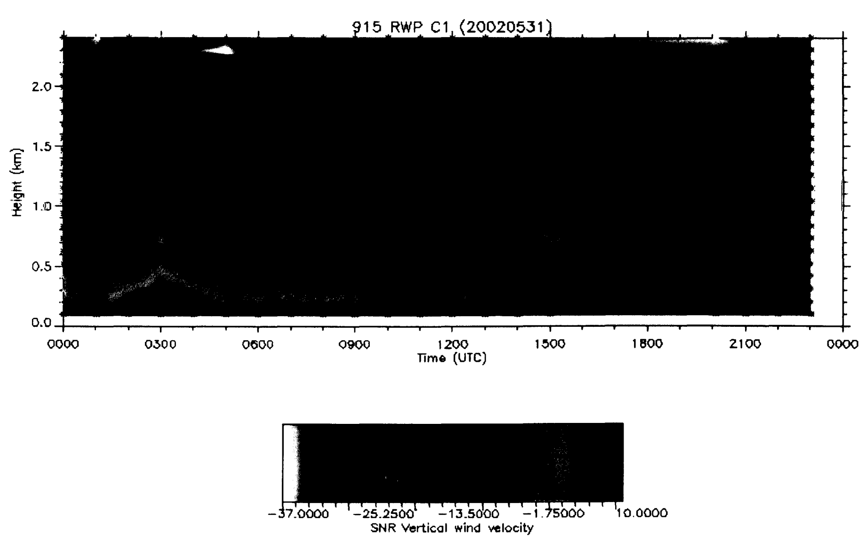

Figure 15: RWP data plot [24]

The MMCR and the SMOS were used indirectly by testing for the presence of clouds and precipitation. An example of the data taken by the MMCR on May 24, 2002 is shown in Fig. (16) at the SGP site.

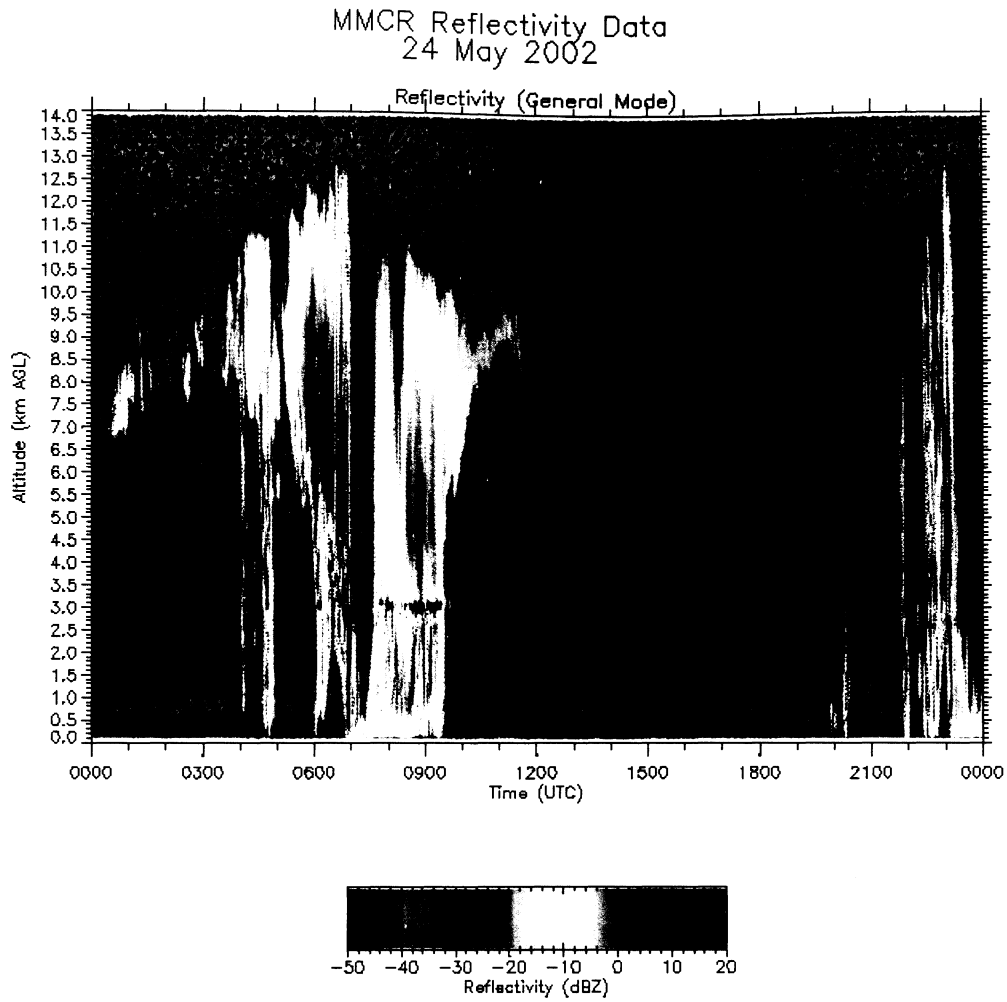

Figure 16: MMCR data plot [25]

Fig. (17) shows a typical sample of the data recorded by the SMOS instrument that includes precipitation, RH, barometric pressure etc.

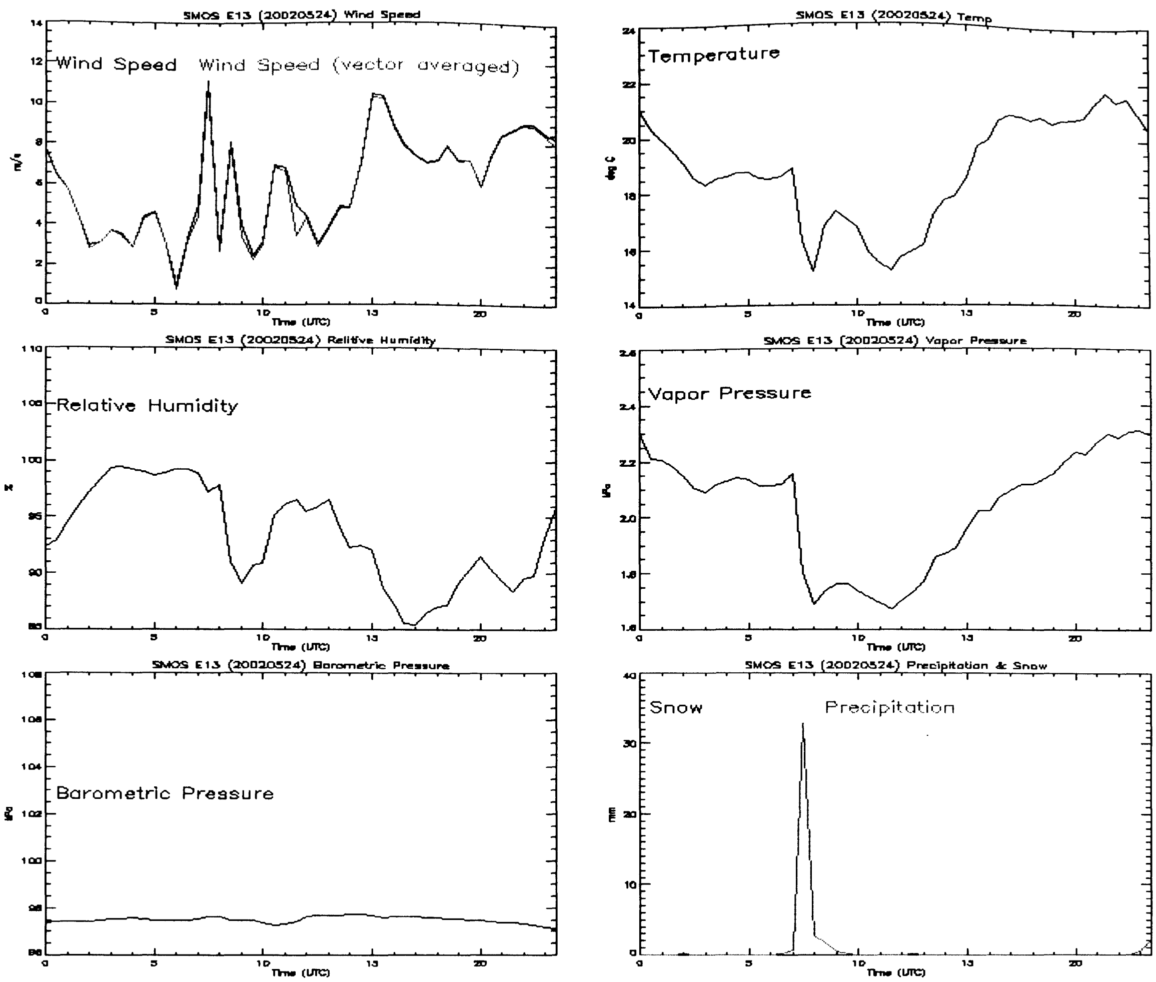

Figure 17: SMOS data plot [26]

Table (8) lists sample data taken from the Southern Great Plains (SGP) site in Lamont, Oklahoma over a period of 4 months. The sample data covers a range of CAPE data. In Table (8) CAPE values are given from days without clouds, with clouds, and days that produced storms with precipitation. The accuracy of the CAPE value is dependent upon the accuracy of the temperature reading of the radiosonde, which is ± 0.5 °C. By taking the average reading of the CAPE over the entire data set, the average accuracy is ± 150 J kg^{-1} of the average CAPE. The accuracy of the RWP velocity is given on the instruments data page website [24].

Table 8: Sample of CAPE/RWP Readings

Date	**Z-Time**	**CAPE (J/kg) ± 150 J/kg**	**RWP(m/s) ± 0.75m/s**
20010611	1126	948	22
20010808	1729	152	11
20010828	2328	1075	26
20010627	1130	1150	35
20010608	528	1528	30
20010825	2328	1544	26
20010612	2029	2106	33
20010611	2030	2321	33
20010621	528	2047	32
20010921	533	1671	35

There were three different independent methods for obtaining vertical velocity. Based on the overall accuracy of each method the standard for statistical comparison was determined. In order to achieve this the average uncertainty for each method used to find velocity was found. The average uncertainty of V_{CAPE} is ± 5.55 m s^{-1} taken from the average velocity calculated from the entire data, which is 55.47 m s^{-1}. The RWP has an uncertainty in each measurement of ± 0.75 m s^{-1}. Calculating the total average uncertainty for the data points results in an average uncertainty of ± .11 m s^{-1}. Since this value is smaller than the original uncertainty, ±0.75 m s^{-1} will be used as the uncertainty of the RWP velocity measurement. The uncertainty with the Brunt-Väisälä velocity includes the uncertainty from the V_{CAPE} as it also depends upon temperature. There is an added uncertainty in the height component of the Brunt-Väisälä equation which when calculated gives an uncertainty of ± 1.5 m s^{-1}. The average Brunt-Väisälä velocity is 14.2 m s^{-1}. From the uncertainties the vertical velocity measured by the RWP is the most accurate of the three methods and therefore it will be used as the standard for the statistical comparison for the CAPE and the Brunt-Väisälä velocity.

The velocity from the CAPE values was calculated from Eq. (8.1) as an energy integration of the Navier-Stokes equations in the absence of friction, as shown in Table (9).

Table 9: Calculated Velocity from CAPE

Date	CAPE	V_{CAPE} (m/s) ± 5.55 m/s
20010611	948	43.5
20010808	152	17.4
20010828	1075	46.4
20010627	1150	47.9
20010608	1528	55.3
20010825	1544	55.6
20010612	2106	64.9
20010611	2321	68.1
20010621	2047	64.0
20010921	1671	57.8

Plotting the RWP velocity and the V_{CAPE} shows the initial differences between the two measurements, Fig. (18).

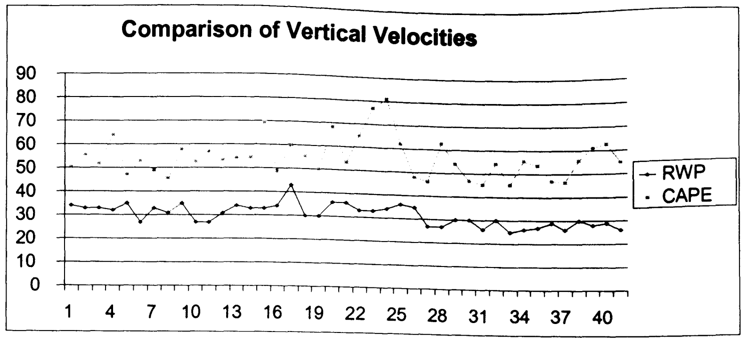

Figure 18: Comparison of vertical velocities from RWP and V_{CAPE}

Taking the velocity calculated from CAPE, the deviations between the RWP value and CAPE values were analyzed, Table (10).

Table 10: Deviation between RWP and V_{CAPE}

Date	**V_{CAPE} (m/s)**	**RWP(m/s)**	**Deviation(RWP-V_{CAPE})**
20010611	43.5	22	-21.5
20010808	17.4	11	-6.4
20010828	46.4	26	-20.4
20010627	47.9	35	-12.9
20010608	55.3	30	-25.3
20010825	55.6	26	-29.3
20010612	64.9	33	-31.9
20010611	68.1	33	-35.1
20010621	64.0	32	-32
20010921	57.8	35	-22.8

The deviations in Table (10) between the RWP and the V_{CAPE} are significant. The average deviation for all the data collected was -24.4 m s^{-1}

and the average RWP for all the data is 31.0 m s^{-1}. The initial assumption that the air parcel ascends adiabatically and behaves as an ideal gas cannot be correct as the deviations show. Therefore CAPE is not completely converted into kinetic energy. "Due to water loading, mixing, entrainment, and evaporative cooling, the actual *w*-max is approximately one-half that calculated above" [27], where we have *w* - max equaling V_{CAPE}. By introducing a CAPE variational condensation parameter *b* in which V_{CAPE} now becomes bV_{CAPE} the energy loss can be accounted for. The objective is to determine the best value of *b* such that the deviations between V_{CAPE} and RWP are insignificant. By doing this a drop in the deviation between RWP and V_{CAPE} can be seen. Fig. (19) is the plot comparing the RWP velocities and the adjusted $0.5V_{CAPE}$ value

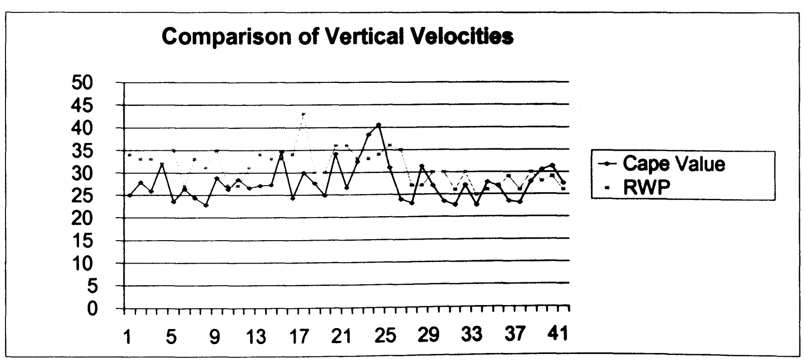

Figure 19: Comparison of RWP velocities and $0.5V_{CAPE}$

Table 11: Deviation between **RWP** and $0.5V_{CAPE}$

Date	$0.5V_{CAPE}$ (m/s)	RWP(m/s)	Deviation(RWP- $0.5V_{CAPE}$)
20010611	21.75	22	.25
20010808	8.7	11	2.3
20010828	23.2	26	2.8
20010627	23.95	35	11.05
20010608	27.65	30	2.35
20010825	27.8	26	-1.8
20010612	32.45	33	.55
20010611	34.0	33	-1.0
20010621	32.0	32	0
20010921	28.9	35	6.1

Overall the data taken, there was an average deviation of 3.33 m s^{-1} between the RWP and the $0.5V_{CAPE}$. A comparative statistical analysis for comparing independent data is shown in Table (12).

Table (12): Statistical analysis for comparing data [28].

1 -- Arithmetic Mean

$$\bar{x} = \frac{1}{N}\sum_{i=1}^{N} x_i \quad (8.3)$$

2 -- Standard Deviation Eq.

$$\sigma_x = \sqrt{\frac{1}{N-1}\sum (x_i - \bar{x})^2} \quad (8.4)$$

3 -- Normal Distribution

$$f_{\bar{x},\sigma}(x) = \frac{1}{\sigma\sqrt{2\pi}} e^{-(x-\bar{x})^2/2\sigma^2} \quad (8.5)$$

4 -- Skewness

$$S = \frac{\sum_{i=1}^{N} (x_i - \bar{x})^3}{(N-1)\sigma^3} \quad (8.6)$$

5 -- Kurtosis

$$K = \frac{\sum_{i=1}^{N} (x_i - \bar{x})^4}{(N-1)\sigma^4} \qquad (8.7)$$

6 -- Chi Squared, χ^2

$$\chi^2 = \sum_{k=1}^{N} \frac{(O_k - E_k)^2}{E_k} \qquad (8.8)$$

7 -- Linear Correlation

$$r = \frac{\sum (x_i - \bar{x})(y_i - \bar{y})}{[\sum (x_i - \bar{x})^2 \sum (y_i - \bar{y})^2]^{1/2}} \qquad (8.9)$$

The mean is the arithmetic average of the all the deviations and the standard deviation is an estimate of the average uncertainty of the measurements. The normal distribution, which is referred to as the Gaussian distribution, is a plot of the frequency of data points that occur within x number of standard deviations. In a Gaussian distribution of 100 data points, 68 are expected to appear within one standard deviation of the mean. For the 41 data point set an expected 28 of the 41 should appear within one standard deviation of the mean. The skewness of a data set indicates if the data is shifted to the right or left of the mean. The kurtosis of a data set indicates how peaked the Gaussian distribution is compared to a true Gaussian distribution. The kurtosis number for a perfect Gaussian distribution is 3. The χ^2 test tests the distributions expected frequency of data to its actual frequency of data. For the data the expected frequency of data appearing within x number of standard deviations is shown in Table (13). The linear correlation gives a value that signifies if the two variables are linearly related. A correlation value of one means the two variables are linearly proportional to each other.

Table 13: Expected frequency of data points

x Standard Deviations from the Mean	-3	-2	-1	1	2	3
Expected Number of Data Points Appearing in the Range	.93	5.57	14	14	5.57	.93

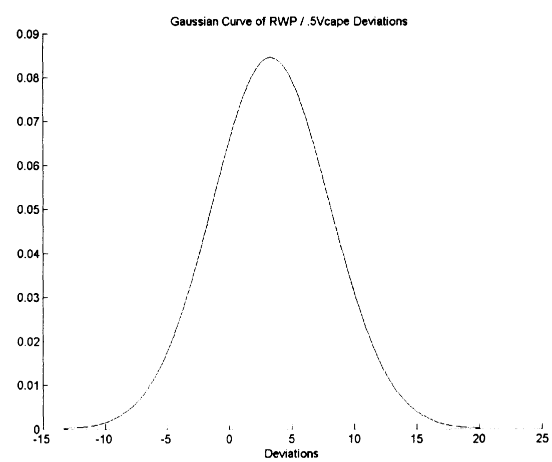

Figure 20: Gaussian distribution of the deviation between the RWP and the $0.5V_{CAPE}$

It is apparent from Fig. (20) that the peak of the curve does not lie above zero, which should occur if the values of the RWP and V_{CAPE} are comparable. The mean for this graph was calculated to be 3.38 m s^{-1} and the standard deviation was calculated to be 4.71. The skewness of the distribution was calculated to be -0.02. Since this number is within one standard deviation the graph is assumed to be asymmetric and Gaussian. In addition to the skewness, the kurtosis of the graph was calculated to be 2.40, which is an acceptable value within the error in the measurements. The χ^2 test results give a value of 0.82 with an expected result of 1. Again the difference can be accounted for in the error of the measurements taken. This indicates that the graph is reasonable close to a Gaussian distribution. Plotting RWP velocity vs. $0.5V_{CAPE}$ a linear correlation of 0.698 as seen from Fig. (21) was obtained. This value indicates that there is not a direct linear correlation between the RWP and the $0.5V_{CAPE}$.

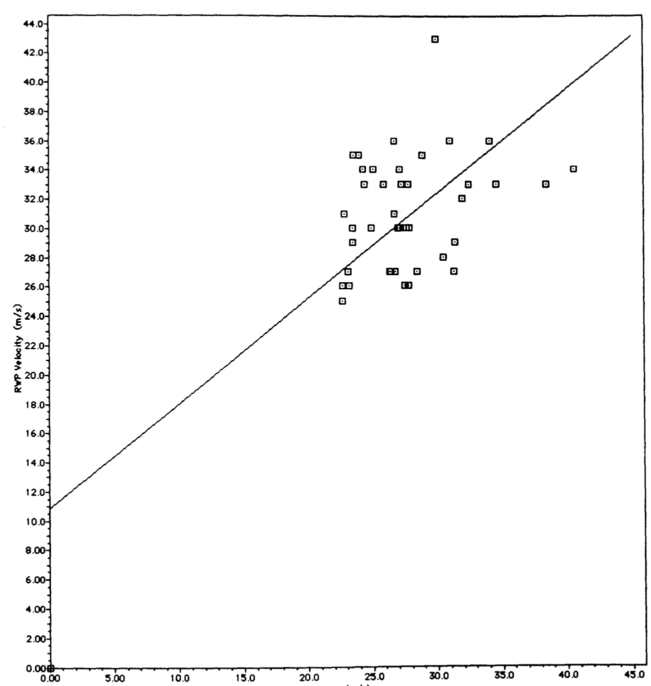

Figure 21: Linear plot of RWP vs. 0.5 V_{CAPE}

It is apparent that $b = 0.5$ is not the best parameter for the data since the deviations do not randomly appear around zero. Picking $b = 0.45$ and applying the same statistical analysis that was done on $b = 0.5$ and compare the bV_{CAPE} to the RWP velocity. Fig. (22) is a plot comparing the RWP velocity and the $0.45V_{CAPE}$.

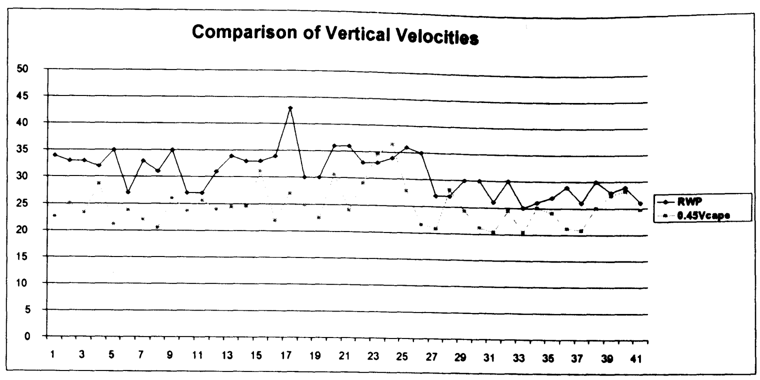

Figure 22: Comparison of RWP velocities and $0.45V_{CAPE}$

Table 14: Deviation between RWP and $0.45V_{CAPE}$

Date	$0.45V_{CAPE}$ (m/s)	RWP(m/s)	Deviation(RWP- $0.45V_{CAPE}$)
20010611	19.6	22	2.4
20010808	7.8	11	3.2
20010828	20.9	26	5.1
20010627	21.6	35	13.4
20010608	24.9	30	5.1
20010825	25.0	26	1.0
20010612	29.2	33	3.8
20010611	30.6	33	2.4
20010621	29.3	32	2.7
20010921	26.0	35	9.0

The Gaussian distribution of the deviations in Table (14) is shown in Fig. (23).

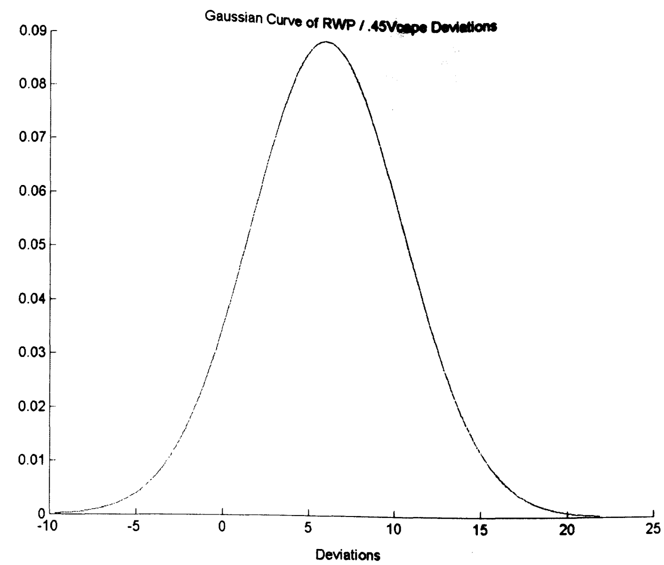

Figure 23: Gaussian distribution of the Deviations between the RWP and the $0.45V_{CAPE}$

The mean of the deviations for the $0.45V_{CAPE}$ and RWP were calculated to be 6.11 and the standard deviation was calculated to be 4.46. The mean for this trial increased which moved the Gaussian distribution away from zero as compared to the $0.5V_{CAPE}$ distribution. The skewness and the kurtosis were calculated to be -0.11 and 2.38 respectively. Both of these numbers are reasonable with the errors involved. The χ^2 test results gave a value of 0.89, which is closer to 1 then the result of the $0.5V_{CAPE}$ test and indicates that this data is also a Gaussian distribution. Plotting RWP vs. $0.45\ V_{CAPE}$ gives a linear correlation of 0.698 as seen from Fig. (24).

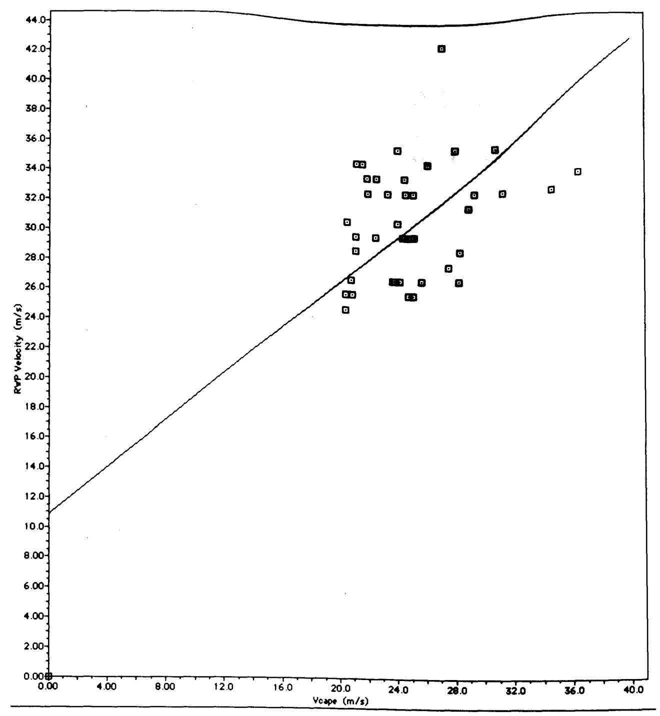

Figure 24: Linear plot of RWP vs. 0.45 V_{CAPE}

Since the $b = 0.45$ parameter shifted the distribution away from zero, the next parameter examined was $b = 0.55$. Fig. (25) compares the RWP velocities to the $0.55V_{CAPE}$. The results of this parameter are shown in Table (15).

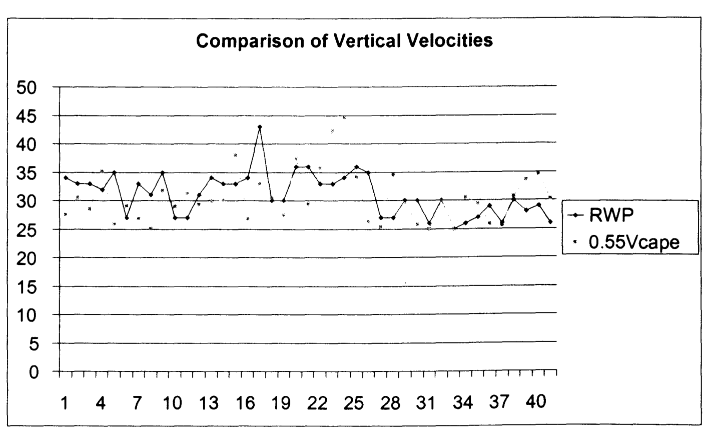

Figure 25: Comparison of RWP velocity and $0.55V_{CAPE}$

Table 15: Deviations between RWP and 0.55 V_{CAPE}

Date	0.55V_{CAPE} (m/s)	RWP(m/s)	Deviation(RWP-0.55V_{CAPE})
20010611	23.9	22	-1.9
20010808	9.6	11	1.4
20010828	25.5	26	0.5
20010627	26.3	35	8.7
20010608	30.4	30	-0.4
20010825	30.6	26	-4.6
20010612	35.7	33	-2.7
20010611	37.5	33	-4.5
20010621	35.2	32	-3.2
20010921	31.8	35	3.2

The mean deviation for the 0.55V_{CAPE} data is 0.56 m s^{-1} and the standard deviation is 4.99. The Gaussian distribution of the deviations in Table (15) is shown in Fig. (26).

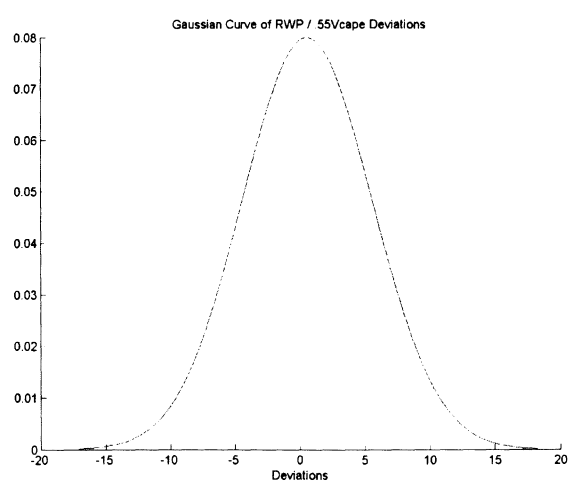

Figure 26: Gaussian distribution of the deviations between the RWP and the 0.55 V_{CAPE}

Calculating the skewness and the kurtosis of the data gives -0.15 and 2.47 respectively. Again these numbers are within an accepted range considering the errors of the measurements. The χ^2 test results give 0.81, which indicates that this is a Gaussian distribution. Plotting RWP vs. $0.55V_{CAPE}$ gives a linear correlation of 0.698 as shown in Fig. (27).

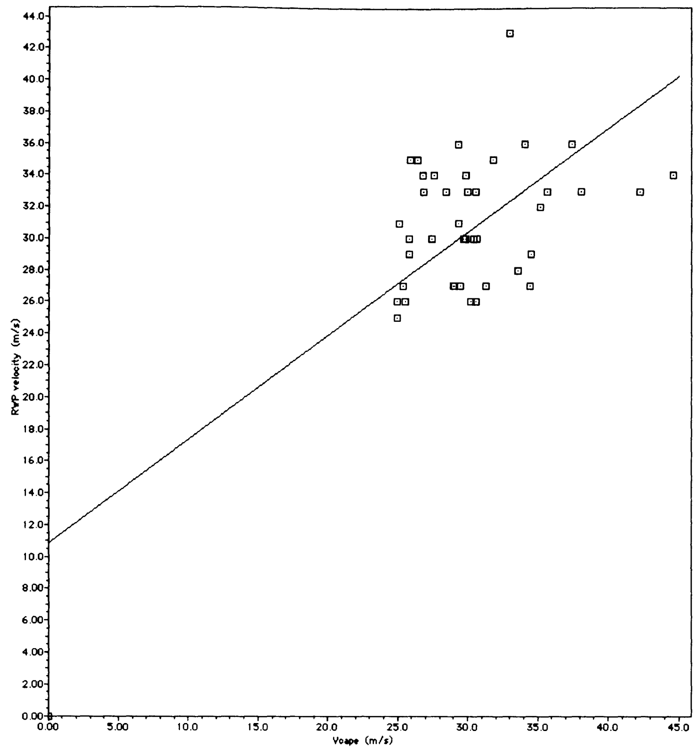

Figure 27: Linear plot of RWP vs. 0.55 V_{CAPE}

All of the three linear correlation values given in Figs. (20), (23), and (26) have the same linear correlation number. However, $b = 0.55$ gives the best fit for a Gaussian distribution as well as the smallest average deviation from the RWP velocity.

The Brunt-Väisälä velocity equation is a different theoretical way of predicting the vertical velocity of the air parcel, Eq. (8.2). The vertical velocities calculated from Eq. (8.2) for the sample data are shown in Table (16).

Table 16: Vertical velocity calculated from the Brunt-Väisälä frequency equation

Date	Brunt-Väisälä Frequency (rad/s)	B-V Velocity (m/s)
20010611	0.009941	12.2
20010808	0.012101	5.31
20010828	0.010150	13.4
20010627	0.010972	15.7
20010608	0.010573	17.0
20010825	0.010341	14.3
20010612	0.011373	17.3
20010611	0.009520	10.5
20010621	0.009990	17.4
20010921	0.011822	17.0

Table (17) shows the deviations calculated from the RWP and the Brunt-Väisälä velocity.

Table 17: Deviations of RWP and Brunt-Väisälä velocity

Date	B-V Velocity	RWP	Deviations (RWP-B-V Velocity)
20010611	12.2	22	9.8
20010808	5.31	11	5.7
20010828	13.4	26	12.6
20010627	15.7	35	19.3
20010608	17.0	30	13.0
20010825	14.3	26	11.7
20010612	17.3	33	15.7
20010611	10.5	33	22.5
20010621	17.4	32	14.6
20010921	17.0	35	18.0

The average deviation between the RWP velocity and the Brunt-Väisälä velocity is 16.8 m s^{-1} with a standard deviation of 5.54. Fig. (28) shows the Gaussian distribution of the deviations calculated for the entire data set.

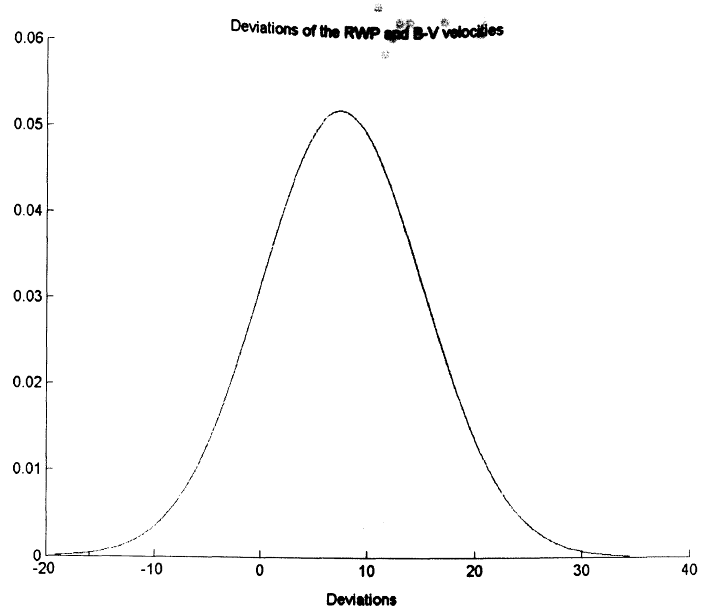

Figure 28: Gaussian distribution of the deviations between the RWP and the Brunt-Väisälä velocity

The skewness and kurtosis of the deviations are 0.14 and 2.85respectively. The χ^2 test result is 0.889 that indicates that the deviations are Gaussian. Plotting RWP vs. Brunt-Väisälä velocity gives a linear correlation of 0.43 as shown in Fig. (29). With the value of the linear correlation it indicates that the RWP and the Brunt-Väisälä velocities are not linearly proportional to each other.

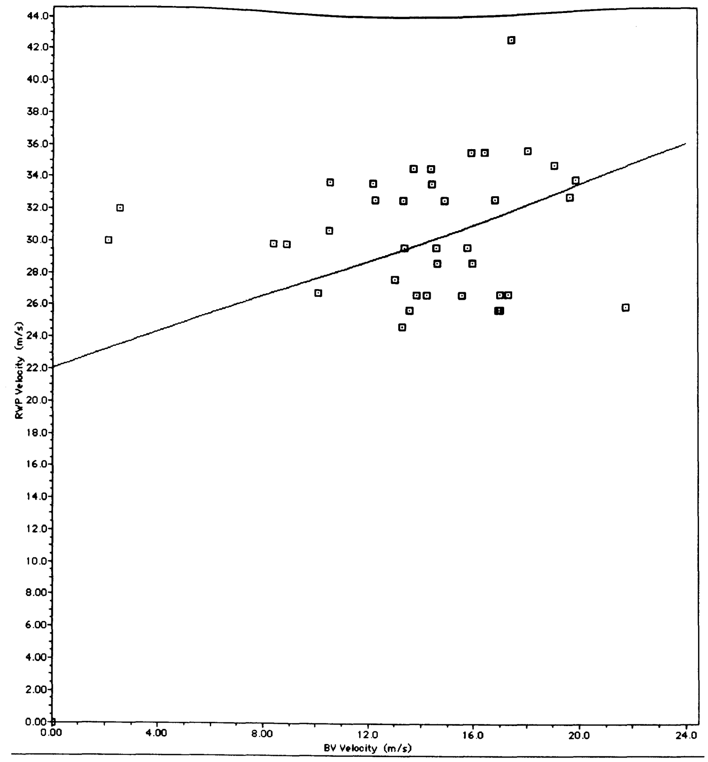

Figure 29: Linear plot of RWP vs. Brunt-Väisälä velocities

Following the study of Williams and Renno [29] the CAPE values over the time period are plotted in a histogram showing the frequency of the CAPE values for this period, Fig. (30). It can be seen that the CAPE values decrease exponentially as the CAPE values increase, which is a special form of a gamma distribution given by

$$f(x) = \frac{1}{\beta} e^{-(x-\mu)/\beta} \tag{8.10}$$

where β is a scale parameter and μ a location parameter [30]. This result is consistent with those of Williams and Renno whose study included topographical locations such as Darwin, Australia and Belém, South America [29]

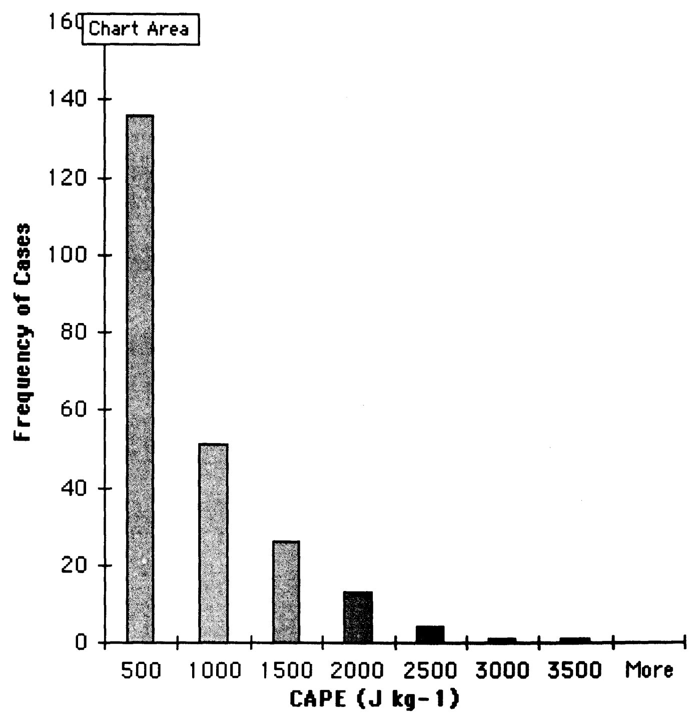

Figure 30: CAPE histograms for soundings at the SGP site

Other methods of evaluating the vertical velocity component of an air parcel are concurrently being studied. These methods include the study of NCAPE and SCAPE, slantwise convective available potential energy, [31]. The NCAPE values for the data taken for CAPE >1000 J kg^{-1} are shown in Appendix C. To date, analysis of the SCAPE has not been found to be as useful [31]. There are days that involve Intense Observation Periods (IOP) in which a BBSS is launched every 10 minutes and the data collected and analyzed in greater detail than days in which the BBSS is sent up only four times a day.

Chapter 9: Conclusions

Vertical velocity profiles have been examined based on thermodynamic, radar, and electronic observations. The velocities of the air parcels were calculated using the CAPE, Brunt-Väisälä frequency, and by direct measurement from the RWP. From the data the velocity determined by the Brunt-Väisälä frequency show an average deviation of 16.8 m s^{-1} with a linear correlation of 0.430. The corrected CAPE values statistically agree with the RWP. Plotting a graph of the average deviation vs. the *b* parameter and finding the equation of best fit leads us to a value of *b* that can be used in the dynamic models of the weather for the SGP site, Fig. (31).

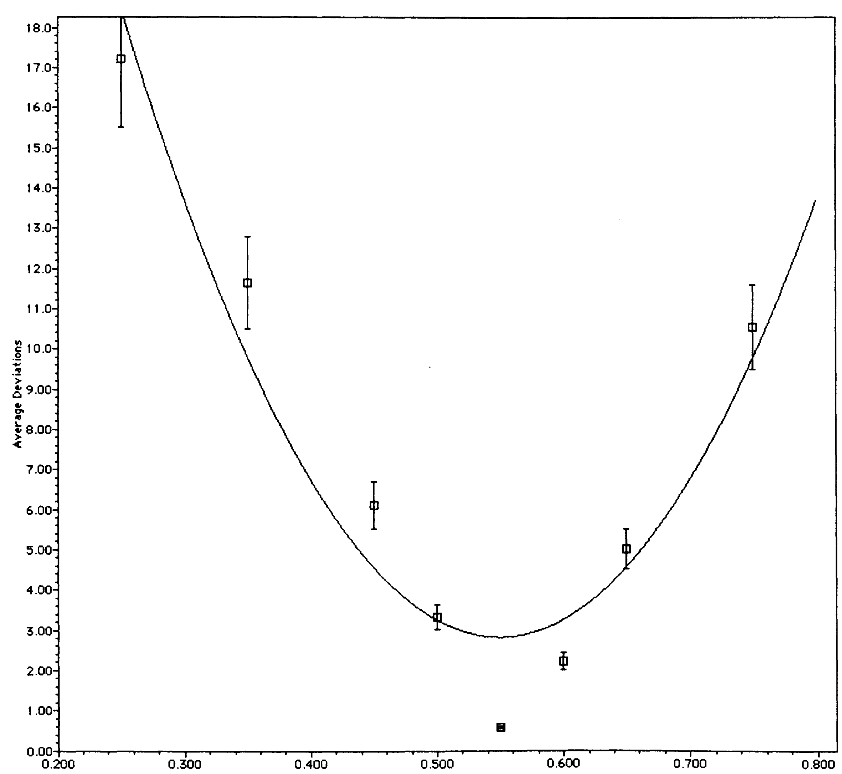

Figure 31: Graph of average deviations vs. *b* parameters

The equation of best fit in Fig. (31) is given by

$$y = 175x^2 - 192x + 55.7. \quad (9.1)$$

Taking the derivative of Eq. (9.1) to find the minimum value that x obtains gives

$$\frac{dy}{dx} = 350x - 192 = 0. \quad (9.2)$$

Solving for x returns a value of 0.549. This is the value of the parameter *b* in the corrected CAPE velocity equations. The data showed when $b = 0.55$ the calculated average deviation was 0.56 m s^{-1} with a linear correlation of 0.698. This parameter $b = 0.55$ in the equation bV_{CAPE} for the SGP site will be helpful in making a dynamic model of the weather around Lamont, Oklahoma.

The current goal of dynamic weather analysis is to predict when severe weather will appear before the storm strikes. When the ability to solve the Navier-Stokes equations becomes available, more accurate weather prediction is likely to occur. Until that time weather prediction will be based on *in situ* data and years of statistical weather information.

Bibliography

1. Bruce Welsh, *A Short History of Meteorology,* Indiana State University, http://isu.indstate.edu/welsh/ua/hist-metro.html, (2002).

2. John M. Wallace, P.V. Hobbs, *Atmospheric Science: An Introductory Survey*, Academic Press, (1977).

3. Steve Kempler, *Atmospheric Structure*, NASA, http://daac.gsfc.nasa.gov/CAMPAIGN_DOCS/ATM_CHEM, (2000).

4. Raymond A. Serway, R.J. Beichner, *Physics: For Scientists and Engineers Fifth Edition*, Saunders College Publishing, (2000).

5. F. Reif, *Fundamentals of Statistical and Thermal Physics*, McGraw-Hill Book Company, (1965).

6. Other more realistic equations of state are given by the van der Waals equation given by $\left(P + \frac{a}{v^2}\right)(v - b) = RT$.

7. Francis W. Sears, Gerhard L. Salinger, *Thermodynamics, Kinetic Theory, and Statistical Thermodynamics: Third Edition*, Addison-Wesley Publishing Company, (1986).

8. Stanley David Gedzelman, *The Science and Wonders of the Atmosphere,* John Wiley & Sons, (1980).

9. National Science Digital Library, *Balloon Borne Sounding System Quicklook Data*, http://nsdl.arm.gov, (2002).

10. Ohio State University Atmospheric Science Program, *Skew-T Thermodynamic Diagram Help,* http://twister.sbs.ohio-state.edu/helpdocs/skew_T_help.html, (1999).

11. John A. Dutton, *Dynamics of Atmospheric Motion,* Dover Publications, Inc. (1986).

12. Ryan Knutsvig, *Severe Weather Indices*, University of North Dakota, http://people.aero.und.edu/~knutsvig/swx2.html, (2000).

13. H.B. Bluestein, *Synoptic-Dynamic Meteorology in Midlatitudes*, Oxford University Press, (1993).

14. D. Djuric, *Weather Analysis*, Prentice-Hall Inc., (1994).

15. Alexander Tardy, *Using Normalized Convective Available Potential Energy to Forecast Moist Convection in Northern California*, Western Region Technical Attachment No. 01-07, available from http://www.wrh.noaa.gov/wrhq/01TAs/0107, (2001).

16. Edward J. Hopkins, *Radiosondes—An Upper Air Probe*, University of Wisconsin Madison, http://www.aos.wisc.edu/~hopkins/wx-inst/wxi-raob.htm, (1996).

17. Atmospheric Radiation Measurement Program, *Tools for the Atmospheric Scientist,* http://www.ux1.eiu.edu/~cxtdm/met/bbss.html

18. Dr. Barry M. Lesht, *Balloon Borne Sounding System,* Argonne National Laboratory, http://www.arm.gov/instruments/static/bbss.html, (2002).

19. Richard L. Coulter, *Radar Wind Profiler and Rass (RW50)*, Argonne National Laboratory, http://www.arm.gov/docs/instruments/static/rwp.html, (2002).

20. Richard L. Coulter, *Radar Wind Profiler and Rass (RWP915),* Argonne National Laboratory, http://www.arm.gov/docs/instruments/static/rwpr.html, (2002).

21. USA Today Website, http://www.usatoday.com/weather/wtipgage.htm, (1999).

22. Kevin Widener, *Millimeter Cloud Radar,* Pacific Northwest National Laboratory, http://www.arm.gov/docs/instruments/static/mmcr.html, (2002).

23. When solving for velocity for a simple harmonic oscillator it is common to use the Root Mean Square of the velocity that equals 0.707 of the maximum velocity. In this study, it is the maximum velocities that are being compared, Eq. (8.2) gives v-max.

24. National Science Digital Library, *Rass / Radar Wind Profiler Quicklook Data*, http://www.nsdl.arm.gov, (2002).

25. National Science Digital Library, *Millimeter Cloud Radar Quicklook Data*, http://www.nsdl.arm.gov, (2002).

26. National Science Digital Library, *Surface Meteorological Observational System Quicklook Data*, http://www.nsdl.arm.gov, (2002).

27. Ben Quinn, *A Description of Atmospheric Soundings: Understanding the Indices of Soundings, and forecasting/predicting severe weather*, Northeast Media of Atmospheric Science Website, wysiwyg://2http://www.nemas.net/edu/soundings/soundings.htm, (2000).

28. John R. Taylor, *An Introduction to Error Analysis*, University Science Books, (1982).

29. Earle Williams and Nilton Renno, "An Analysis of the Conditional Instability of the Tropical Atmosphere", *American Meteorological Society*, **121**, 21 (1993).

30. National Institute of Standards and Technology, *Exponential Distribution*, http://www.itl.nist.gov/div898/handbook/eda/section3/eda3667.htm, (2002).

31. Charles A. Doswell III, et. al, "The Intricacies of Instabilities", *American Meteorological Society*, **128**, 4143 (2000).

Appendix A: Derivations of Eq. (3.1), (3.2), and (3.3) [4]

From Fig. (5) a molecule is shown colliding into one of the sides of a container. Due to conservation of momentum the total momentum during an elastic collision of a system before equals the total momentum after the collision. Examining the conservation of momentum in the x direction gives a total change of momentum equal to

$$\Delta p_x = p_{xf} - p_{xi} = -mv_x - mv_x = -2mv_x . \qquad (A.1)$$

If the molecule is going to collide twice with the same wall it must travel a distance of 2d in the x direction. The time that it takes for the molecule to complete the two collisions is $\Delta t = 2d/ v_x$. From the Impulse-momentum theorem the force that is acting on this molecule during the time of impact is equal to

$$F = \frac{\Delta p_x}{\Delta t} = \frac{-2mv_x}{\Delta t} = \frac{-2mv_x}{2d/v_x} = \frac{-mv_x^2}{d}. \qquad (A.2)$$

From Newton's third law the force that the molecule exerts on the wall is equal and opposite of Eq. (A.2); therefore the molecule exerts a force on the wall equal to

$$F_{1onwall} = \frac{mv_x^2}{d}. \qquad (A.3)$$

This force is from only one molecule hitting the wall. To find the total force exerted on the wall by all the molecules in the x direction, all the forces from each individual molecule must be summed together. Since the assumption in Chapter 3 was that all the molecules were identical, m is the same for all the molecules as well as the distance d each one has to travel. Therefore, it is the velocities that can differ in the x direction. To find the total force, the average value of the square of the velocities in the x direction is calculated and that result is substituted into Eq. (A.3), which gives

$$F = \frac{Nm}{d}\overline{v}_x^2 \tag{A.4}$$

where N is the total number of molecules in the container and v-bar squared is the average value of the square of the velocities in the x direction.

In order to find the total force acting on the container from all three directions the velocities of each molecule in each direction must be known. If one molecule has a velocity in the x, y, and z directions then the total velocity of the molecule v is related by

$$v^2 = v_x^2 + v_y^2 + v_z^2 \tag{A.5}$$

according to Pythagorean's theorem. Since all the molecules in the container have to be considered, the average of each molecule must be taken

$$\overline{v}^2 = \overline{v}_x^2 + \overline{v}_y^2 + \overline{v}_z^2. \tag{A.6}$$

Since the motion of the molecules is random, the average velocities in each direction will be equal to the average velocity in the x direction. Because of this Eq. (A.6) becomes

$$\bar{v}^2 = 3\bar{v}_x^2 \qquad (A.7)$$

which leads to the total force acting on the walls of the container to be

$$F = \frac{N}{3}\left(\frac{m\bar{v}^2}{d}\right). \qquad (A.8)$$

Plugging Eq. (A.8) into the definition of pressure a form of the ideal gas law can be derived.

$$P = \frac{F}{A} = \frac{N}{3}\left(\frac{m\bar{v}^2}{d^3}\right) = \frac{N}{3}\left(\frac{m\bar{v}^2}{V}\right)$$

$$PV = \frac{N}{3}m\bar{v}^2 \qquad (A.9)$$

Appendix B: Data Tables

	Date	Time	CAPE	Vertical Velocity (RWP)	V-CAPE	Difference between RWP and V-CAPE	0.5V-CAPE	Difference Between RWP and 0.5V-CAPE	0.45V-CAPE	Difference Between RWP and 0.45V-CAPE	0.55V-CAPE	Difference Between RWP and 0.55V-CAPE
*	20010614	530	1258	34	50.16	-16.16	25.08	8.92	22.57	11.43	27.59	6.41
*	20010620	2106	1548	33	55.64	-22.64	27.82	5.18	25.04	7.96	30.60	2.40
*	20010620	2329	1341	33	51.79	-18.79	25.89	7.11	23.30	9.70	28.48	4.52
*	20010621	528	2047	32	63.98	-31.98	31.99	0.01	28.79	3.21	35.19	-3.19
*	20010628	2028	1109	35	47.10	-12.10	23.55	11.45	21.19	13.81	25.90	9.10
*	20010907	528	1395	27	52.82	-25.82	26.41	0.59	23.77	3.23	29.05	-2.05
*	20010917	528	1192	33	48.83	-15.83	24.41	8.59	21.97	11.03	26.85	6.15
*	20010917	2328	1040	31	45.61	-14.61	22.80	8.20	20.52	10.48	25.08	5.92
*	20010921	533	1671	35	57.81	-22.81	28.91	6.09	26.01	8.99	31.80	3.20
*	20010921	1136	1384	27	52.61	-25.61	26.31	0.69	23.68	3.32	28.94	-1.94
*	20010922	2339	1621	27	56.94	-29.94	28.47	-1.47	25.62	1.38	31.32	-4.32
*	20010922	1739	1423	31	53.35	-22.35	26.67	4.33	24.01	6.99	29.34	1.66
	20010602	1130	1472	34	54.26	-20.26	27.13	6.87	24.42	9.58	29.84	4.16
	20010603	528	1485	33	54.50	-21.50	27.25	5.75	24.52	8.48	29.97	3.03
	20010603	1127	2396	33	69.22	-36.22	34.61	-1.61	31.15	1.85	38.07	-5.07
	20010604	533	1182	34	48.62	-14.62	24.31	9.69	21.88	12.12	26.74	7.26
	20010605	2329	1797	43	59.95	-16.95	29.97	13.03	26.98	16.02	32.97	10.03
	20010608	533	1528	30	55.28	-25.28	27.64	2.36	24.88	5.12	30.40	-0.40
	20010608	1130	1246	30	49.92	-19.92	24.96	5.04	22.46	7.54	27.46	2.54
	20010611	2030	2321	36	68.13	-32.13	34.07	1.93	30.66	5.34	37.47	-1.47
	20010611	2330	1423	36	53.35	-17.35	26.67	9.33	24.01	11.99	29.34	6.66
	20010612	2029	2106	33	64.90	-31.90	32.45	0.55	29.20	3.80	35.69	-2.69
	20010612	2329	2956	33	76.89	-43.89	38.44	-5.44	34.60	-1.60	42.29	-9.29
	20010613	2030	3291	34	81.13	-47.13	40.56	-6.56	36.51	-2.51	44.62	-10.62
	20010616	2330	1922	36	62.00	-26.00	31.00	5.00	27.90	8.10	34.10	1.90
	20010627	1130	1150	35	47.96	-12.96	23.98	11.02	21.58	13.42	26.38	8.62
	20010801	2327	1068	27	46.22	-19.22	23.11	3.89	20.80	6.20	25.42	1.58
	20010806	1728	1959	27	62.59	-35.59	31.30	-4.30	28.17	-1.17	34.43	-7.43
	20010817	1126	1459	30	54.02	-24.02	27.01	2.99	24.31	5.69	29.71	0.29
	20010821	1728	1100	30	46.90	-16.90	23.45	6.55	21.11	8.89	25.80	4.20
	20010822	1741	1029	26	45.37	-19.37	22.68	3.32	20.41	5.59	24.95	1.05
	20010824	528	1473	30	54.28	-24.28	27.14	2.86	24.42	5.58	29.85	0.15
	20010824	2329	1027	25	45.32	-20.32	22.66	2.34	20.39	4.61	24.93	0.07
	20010825	2328	1544	26	55.57	-29.57	27.78	-1.78	25.01	0.99	30.56	-4.56
	20010827	1125	1435	27	53.57	-26.57	26.79	0.21	24.11	2.89	29.46	-2.46
	20010828	1129	1102	29	46.95	-17.95	23.47	5.53	21.13	7.87	25.82	3.18
	20010828	2328	1075	26	46.37	-20.37	23.18	2.82	20.87	5.13	25.50	0.50
	20010829	529	1554	30	55.75	-25.75	27.87	2.13	25.09	4.91	30.66	-0.66
	20010903	1722	1862	28	61.02	-33.02	30.51	-2.51	27.46	0.54	33.56	-5.56
	20010920	1740	1966	29	62.71	-33.71	31.35	-2.35	28.22	0.78	34.49	-5.49
	20010923	539	1509	26	54.94	-28.94	27.47	-1.47	24.72	1.28	30.21	-4.21

* Indicates recorded precipitation that day

	Date	Time	CAPE	Vertical Velocity (RWP)	0.65V-CAPE	0.75V-CAPE	0.35V-CAPE	0.25V-CAPE	0.6V-CAPE	Difference Between RWP and 0.75V-CAPE	Difference Between RWP and 0.35V-CAPE	Difference Between RWP and 0.25V-CAPE	Difference Between RWP and 0.6V-CAPE
*	20010614	530	1258	34	32.6038341	37.6198086	17.5559107	12.5399362	30.0958469	-3.6198086	16.4440893	21.4600638	3.90415311
*	20010620	2106	1548	33	36.1671121	41.7312832	19.4745988	13.9104277	33.3850266	-8.7312832	13.5254012	19.0895723	-0.3850266
*	20010620	2329	1341	33	33.6622192	38.8410221	18.1258103	12.9470074	31.0728177	-5.8410221	14.8741897	20.0529926	1.9271823
*	20010621	528	2047	32	41.5898425	47.9882798	22.3945306	15.9960933	38.3906239	-15.98828	9.60546942	16.0039067	-6.3906239
*	20010628	2028	1109	35	30.6121708	35.3217355	16.4834766	11.7739118	28.2573884	-0.3217355	18.5165234	23.2260882	6.74261159
*	20010907	528	1395	27	34.3332929	39.6153379	18.4871577	13.2051126	31.6922704	-12.615338	8.5128423	13.7948874	-4.6922704
*	20010917	528	1192	33	31.7370446	36.6196668	17.0891779	12.2065556	29.2957335	-3.6196668	15.9108221	20.7934444	3.70426652
*	20010917	2328	1040	31	29.6445611	34.2052628	15.962456	11.4017543	27.3642102	-3.2052628	15.037544	19.5982457	3.6357898
*	20010921	533	1671	35	37.5765219	43.3575253	20.2335118	14.4525084	34.6860202	-8.3575253	14.7664882	20.5474916	0.31397976
*	20010921	1136	1384	27	34.1976607	39.4588393	18.414125	13.1529464	31.5670715	-12.458839	8.58587499	13.8470536	-4.5670715
*	20010922	2339	1621	27	37.0100662	42.7039225	19.9284972	14.2346408	34.163138	-15.703923	7.07150282	12.7653592	-7.163138
*	20010922	1739	1423	31	34.6761445	40.010936	18.6717701	13.3369787	32.0087488	-9.010936	12.3282299	17.6630213	-1.0087488
	20010602	1130	1472	34	35.2681159	40.6939799	18.990524	13.56466	32.5551839	-6.6939799	15.009476	20.43534	1.44481608
	20010603	528	1485	33	35.4235091	40.8732798	19.0741972	13.6244266	32.6986238	-7.8732798	13.9258028	19.3755734	0.30137618
	20010603	1127	2396	33	44.9957776	51.9182049	24.2284956	17.3060683	41.5345639	-18.918205	8.77150438	15.6939317	-8.5345639
	20010604	533	1182	34	31.603639	36.4657373	17.0173441	12.1552458	29.1725899	-2.4657373	16.9826559	21.8447542	4.82741013
	20010605	2329	1797	43	38.9674864	44.9624844	20.9824927	14.9874948	35.9699875	-1.9624844	22.0175073	28.0125052	7.03001251
	20010608	533	1528	30	35.9327149	41.4608249	19.3483849	13.820275	33.1686599	-11.460825	10.6516151	16.179725	-3.1686599
	20010608	1130	1246	30	32.4479583	37.4399519	17.4719776	12.479984	29.9519615	-7.4399519	12.5280224	17.520016	0.04803846
	20010611	2030	2321	36	44.2859459	51.0991683	23.8462785	17.0330561	40.8793346	-15.099168	12.1537215	18.9669439	-4.8793346
	20010611	2330	1423	36	34.6761445	40.010936	18.6717701	13.3369787	32.0087488	-4.010936	17.3282299	22.6630213	3.9912512
	20010612	2029	2106	33	42.1849499	48.6749422	22.714973	16.2249807	38.9399538	-15.674942	10.285027	16.7750193	-5.9399538
	20010612	2329	2956	33	49.9781952	57.6671484	26.9113359	19.2223828	46.1337187	-24.667148	6.0886641	13.7776172	-13.133719
	20010613	2030	3291	34	52.7341919	60.8471446	28.3953341	20.2823815	48.6777156	-26.847145	5.60466588	13.7176185	-14.677716
	20010616	2330	1922	36	40.3	46.5	21.7	15.5	37.2	-10.5	14.3	20.5	-1.2
	20010627	1130	1150	35	31.1729049	35.9687364	16.7854103	11.9895788	28.7749891	-0.9687364	18.2145897	23.0104212	6.22501086
	20010801	2327	1068	27	30.040972	34.66266	16.175908	11.55422	27.730128	-7.66266	10.824092	15.44578	-0.730128
	20010806	1728	1959	27	40.6860541	46.9454471	21.9078753	15.6484824	37.5563577	-19.945447	5.0921247	11.3515176	-10.556358
	20010817	1126	1469	30	35.112035	40.5138865	18.9064804	13.5046288	32.4111092	-10.513887	11.0935196	16.4953712	-2.4111092
	20010821	1728	1100	30	30.4877024	35.1781182	16.4164552	11.7260394	28.1424946	-5.1781182	13.5835448	18.2739606	1.85750544
	20010822	1741	1029	26	29.4873702	34.0238887	15.8778147	11.3412962	27.2191109	-8.0238887	10.1221853	14.6587038	-1.2191109
	20010824	528	1473	30	35.2800935	40.7078002	18.9969734	13.5692667	32.5662402	-10.7078	11.0030266	16.4307333	-2.5662402
	20010824	2329	1027	25	29.4586999	33.9908076	15.8623769	11.3302692	27.1926461	-8.9908076	9.13762313	13.6697308	-2.1926461
	20010825	2328	1544	26	36.1203544	41.677332	19.4494216	13.892444	33.3418656	-15.677332	6.55057841	12.107556	-7.3418656
	20010827	1125	1435	27	34.8220476	40.1792857	18.7503333	13.3930952	32.1434286	-13.179286	8.24966667	13.6069048	-5.1434286
	20010828	1129	1102	29	30.5154059	35.2100838	16.4313724	11.7366946	28.168067	-6.2100838	12.5686276	17.2633054	0.83193297
	20010828	2328	1075	26	30.1392601	34.7760694	16.2288324	11.5920231	27.8208555	-8.7760694	9.77116763	14.4079769	-1.8208555
	20010829	529	1554	30	36.2371356	41.8120796	19.5123038	13.9373599	33.4496637	-11.81208	10.4876962	16.0626401	-3.4496637
	20010903	1722	1862	28	39.6659804	45.7684389	21.3586048	15.2561463	36.6147511	-17.768439	6.64139518	12.7438537	-8.6147511
	20010920	1740	1966	29	40.7586801	47.0292462	21.9469816	15.6764154	37.623397	-18.029246	7.05301843	13.3235846	-8.623397
	20010923	539	1509	26	35.7086124	41.2022451	19.2277144	13.7340817	32.9617961	-15.202245	6.77228563	12.2659183	-6.9617961

	Date	Time	CAPE	Vertical Velocity (RWP)	Velocity fom B-V freq	Difference Between RWP and Brunt-Vaisala Velocity
*	20010614	530	1258	34	19.8925716	14.1074284
*	20010620	2106	1548	33	#DIV/0!	#DIV/0!
*	20010620	2329	1341	33	14.9109864	18.0890136
*	20010621	528	2047	32	2.56389131	29.4361087
*	20010628	2028	1109	35	19.0664057	15.9335943
*	20010907	528	1395	27	17.0135269	9.98647314
*	20010917	528	1192	33	16.7948096	16.2051904
*	20010917	2328	1040	31	10.5210625	20.4789375
*	20010921	533	1671	35	13.7486676	21.2513324
*	20010921	1136	1384	27	17.3337813	9.66621871
*	20010922	2339	1621	27	15.5728864	11.4271136
*	20010922	1739	1423	31	#DIV/0!	#DIV/0!
	20010602	1130	1472	34	12.1986198	21.8013802
	20010603	528	1485	33	#DIV/0!	#DIV/0!
	20010603	1127	2396	33	19.6642703	13.3357297
	20010604	533	1182	34	14.4538735	19.5461265
	20010605	2329	1797	43	17.4289224	25.5710776
	20010608	533	1528	30	15.7454394	14.2545606
	20010608	1130	1246	30	8.38276426	21.6172357
	20010611	2030	2321	36	15.8991965	20.1008035
	20010611	2330	1423	36	18.069003	17.930997
	20010612	2029	2106	33	12.2916068	20.7083932
	20010612	2329	2956	33	13.3583355	19.6416645
	20010613	2030	3291	34	10.5779406	23.4220594
	20010616	2330	1922	36	16.4107903	19.5892097
	20010627	1130	1150	35	14.4146111	20.5853889
	20010801	2327	1068	27	14.2554726	12.7445274
	20010806	1728	1959	27	13.859919	13.140081
	20010817	1126	1459	30	2.14154755	27.8584525
	20010821	1728	1100	30	13.365167	16.634833
	20010822	1741	1029	26	16.9237331	9.0762669
	20010824	528	1473	30	14.5881031	15.4118969
	20010824	2329	1027	25	13.2927935	11.7072065
	20010825	2328	1544	26	21.7664317	4.2335683
	20010827	1125	1435	27	10.1026046	16.8973954
	20010828	1129	1102	29	15.9574335	13.0425665
	20010828	2328	1075	26	17.0069558	8.99304415
	20010829	529	1554	30	8.91507633	21.0849237
	20010903	1722	1862	28	13.0344329	14.9655671
	20010920	1740	1966	29	14.6259229	14.3740771
	20010923	539	1509	26	13.5967771	12.4032229

Appendix C: NCAPE values calculated

	Date	Time	CAPE	NCAPE
*	20010614	530	1258	0.155886
*	20010620	2106	1548	0.136304
*	20010620	2329	1341	0.148719
*	20010621	528	2047	0.186838
*	20010628	2028	1109	0.215801
*	20010907	528	1395	0.184158
*	20010917	528	1192	0.103356
*	20010917	2328	1040	0.184201
*	20010921	533	1671	0.184968
*	20010921	1136	1384	0.177095
*	20010922	2339	1621	0.192632
*	20010922	1739	1423	0.158499
	20010602	1130	1472	0.13081
	20010603	528	1485	0.05178
	20010603	1127	2396	0.246249
	20010604	533	1182	0.795424
	20010605	2329	1797	0.169544
	20010608	533	1528	0.151212
	20010608	1130	1246	0.121336
	20010611	2030	2321	0.334438
	20010611	2330	1423	0.175506
	20010612	2029	2106	0.22004
	20010612	2329	2956	0.320468
	20010613	2030	3291	#DIV/0!
	20010616	2330	1922	#DIV/0!
	20010627	1130	1150	0.127608
	20010801	2327	1068	0.110331
	20010806	1728	1959	0.191402
	20010817	1126	1459	0.20219
	20010821	1728	1100	0.114108
	20010822	1741	1029	0.180495
	20010824	528	1473	0.156852
	20010824	2329	1027	0.123408
	20010825	2328	1544	0.178353
	20010827	1125	1435	0.170894
	20010828	1129	1102	0.649764
	20010828	2328	1075	0.130004
	20010829	529	1554	0.160653
	20010903	1722	1862	0.207789
	20010920	1740	1966	0.205048
	20010923	539	1509	0.177362